

1
2
3 **Poly(3-hydroxyoctanoate), a promising new material for**
4
5
6 **cardiac tissue engineering**
7
8

9
10 *Andrea V. Bagdadi*¹, *Maryam Safari*¹, *Prachi Dubey*¹, *Pooja Basnett*¹, *Panagiotis*
11 *Sofokleous*², *Eleanor Humphrey*⁶, *Ian Locke*¹, *Mohan Edirisinghe*², *Cesare*
12 *Terracciano*⁶, *Aldo R. Boccaccini*³, *Jonathan C. Knowles*^{4,5}, *Sian E. Harding*⁶,
13
14
15 *Ipsita Roy*^{1*}
16
17

- 18
19
20 1. Applied Biotechnology Research Group, Faculty of Science and Technology,
21 University of Westminster, London, UK
22
23 2. Department of Mechanical Engineering, UCL, London, UK
24
25 3. Department of Materials Science and Engineering, University of Erlangen-
26 Nuremberg, Erlangen, Germany
27
28 4. Department of Biomaterials and Tissue engineering, Eastman Dental Institute,
29 UCL, London, UK
30
31 5. Department of Nanobiomedical Science & BK21 Plus NBM Global Research
32 Center for Regenerative Medicine, Dankook University, Republic of Korea
33
34 6. National Heart and Lung Institute, Imperial College, London, UK
35
36
37
38
39
40
41
42

43 *Corresponding author
44

45
46 Professor Ipsita Roy
47

48 Faculty of Science and Technology
49

50 University of Westminster
51

52 115 New Cavendish Street
53
54

55 London W1W 6UW, UK
56
57
58
59
60

Abstract:

Cardiac tissue engineering (CTE) is currently a prime focus of research due to an enormous clinical need. In this work, a novel functional material, Poly(3-hydroxyoctanoate), P(3HO), a medium chain length polyhydroxyalkanoate (PHA), produced using bacterial fermentation, was studied as a new potential material for CTE. Engineered constructs with improved mechanical properties, crucial for supporting the organ during new tissue regeneration, and enhanced surface topography, to allow efficient cell adhesion and proliferation, were fabricated. Our results showed that the mechanical properties of the final patches were close to that of cardiac muscle. Biocompatibility of the P(3HO) neat patches, assessed using Neonatal ventricular rat myocytes (NVRM), showed that the polymer was as good as collagen in terms of cell viability, proliferation and adhesion. Enhanced cell adhesion and proliferation properties were observed when porous and fibrous structures were incorporated to the patches. Also, no deleterious effect was observed on the adults cardiomyocytes' contraction when cardiomyocytes were seeded on the P(3HO) patches. Hence, P(3HO) based multifunctional cardiac patches are promising constructs for efficient CTE. This work will provide a positive impact on the development of P(3HO) and other PHAs as a novel new family of biodegradable functional materials with huge potential in a range of different biomedical applications, particularly CTE, leading to further interest and exploitation of these materials.

Keywords: Cardiac Tissue Engineering, Polyhydroxyalkanoates, Poly(3-hydroxyoctanoate), cardiac patches

1. Introduction

Cardiovascular diseases (CVDs) are the leading cause of death throughout the world (Morosco 2002, Perry and Roth 2003). According to the World Health Organization, an estimated 17.3 million people died from CVDs in 2008 and it is predicted that by 2030 almost 25 million people will die from CVDs. Myocardial infarction is the main cause of death in patients with CVDs. The acute loss of myocardium triggers a cascade of cell signals activating a ventricular and early and late remodelling process. The early ventricular remodelling process includes the formation, thinning and elongation of a fibrotic scar that cause elevation of diastolic and systolic wall stresses. An increased wall stress leads to a late remodelling characterized by myocyte hypertrophy and production of interstitial collagen with an increased wall mass and chamber enlargement (Sutton and Shape 2000). Myocardial infarction may eventually lead to the deterioration of systolic or diastolic function and to increased predisposition to arrhythmias and other long-term complications.

The combination of a natural or synthetic biomaterial with relevant cells and growth factors *ex vivo* is currently receiving much attention for cardiac tissue engineering treatments (Giraud *et al.*, 2007). The final goal will be the selection of an appropriate cell type and the development of a biocompatible flexible functional material that stimulates cell growth and guides and supports tissue regeneration in order to replace the formed scar tissue with functioning cardiac muscle tissue. The material's physical and mechanical characteristics should be similar enough to those of the natural myocardium in order to support the organ during the regeneration process, and its composition should allow it to degrade as the new tissue is formed (Jawad *et al.*, 2008). Bioabsorbable polymeric materials provide an extracellular matrix where growing cells can localize and interact to form new tissue. An ideal biomaterial

1
2
3 should possess five special characteristics. First, the material should be
4
5 biocompatible. Second, the material's mechanical properties should be similar to the
6
7 host tissue to provide mechanical support to the cells until the cells synthesize new
8
9 extracellular matrix. As previously described, myocardial infarction normally results
10
11 in wall thinning and ventricular dilatation that causes a significant stress in the heart
12
13 wall. An overstressed wall leads to a progressive ventricular remodelling with an end
14
15 stage of heart failure (Sutton and Shape 2000). In order to prevent an overstressed
16
17 wall with a negative ventricular remodelling, the material's mechanical properties
18
19 should allow reduction of the heart wall stress (Chen *et al.*, 2008). Third, the material
20
21 should possess an appropriate shape and size to guide and organize the cells and to
22
23 repair at the implant site. Fourth, the chemistry of the material's surface should allow
24
25 cell attachment, differentiation and proliferation. Fifth, the composition of the
26
27 material should allow biodegradation *in vivo* at rates appropriate for tissue
28
29 regeneration (Williams *et al.*, 1999).
30
31
32
33

34 In this work we propose Poly(3-hydroxyoctanoate), P(3HO), a medium chain length
35
36 biodegradable and biocompatible polyhydroxyalkanoate, as a novel functional
37
38 healthcare material for application in CTE to deliver cells to the injured tissue and to
39
40 support the heart during its regeneration process. PHAs are polyesters composed of
41
42 several units of hydroxyalkanoate monomers linked to each other through ester
43
44 linkages. Numerous microorganisms synthesize PHAs by the fermentation of a carbon
45
46 source and then accumulate them as intracellular carbon reserve inclusion bodies.
47
48 Previous literature has shown that *Pseudomonas mendocina* produced a unique
49
50 P(3HO) homopolymer when sodium octanoate was used as a sole carbon source with
51
52 an excess supply of carbon and limitation of nitrogen (Rai *et al.*, 2011). The P(3HO)
53
54 homopolymer is a unique candidate for cardiac tissue engineering due to its
55
56
57
58
59
60

1
2
3 biocompatibility, biodegradability and elastomeric properties. One of the main
4 reasons of PHA biocompatibility is the presence of some PHA monomer units in
5 human blood and tissues (Hocking *et al.*, 1994, Nelson *et al.*, 1981). Additionally,
6 PHA biodegradation occurs by erosion from the surface to the interior in contrast to
7 other amorphous polymers such as PLGA, which exhibit bulk degradation (Weng *et*
8 *al.*, 2011). Finally, the combination of P(3HO)'s low crystallinity (37.5%), with Tg
9 values below ambient temperature, imparts to the polymer an elastomeric behaviour
10 crucial to support the organ for synchronised beating (Rai *et al.*, 2011).

11
12
13
14
15
16
17
18
19
20
21 Collagen, as the main constituent of the myocardial extracellular matrix, facilitates
22 cell adhesion and proliferation and maintain cells in their differentiated states because
23 of its particular adhesive properties (Jawad *et al.*, 2008). In this work, in order to
24 understand the P(3HO) biocompatibility and adhesive properties, freshly isolated
25 NVRMs were seeded on both P(3HO) and collagen, and the cell viability was
26 compared.

27
28
29
30
31
32
33
34 An appropriate level of cardiomyocyte contraction is a crucial factor for a highly
35 regulated mechanical system such as the heart, in order to maintain its accurate
36 pumping function. The effect of the P(3HO) polymer on contracting cardiomyocytes
37 was studied by seeding freshly isolated adult cardiomyocytes from rat on P(3HO)
38 patches films.

39
40
41
42
43
44
45 Engineered P(3HO) cardiac patches with appropriate mechanical properties to support
46 the injured organ and to allow cell growth for efficient cell delivery were created. Our
47 first approach was the design of permeable porous structures with pore size
48 comparable to that of cardiomyocytes, with an appropriate surface structure for cell
49 attachment, which permits the ingress of cells and guides their growth, leading to
50 tissue regeneration in three dimensions. Eventually, the polymer matrix would be
51
52
53
54
55
56
57
58
59
60

1
2
3 degraded leaving behind new tissue. In a second approach, as collagen is the main
4
5 constituent of the extracellular matrix and exhibits a distinct fibrous architecture, in
6
7 order to mimic such fibrous structure, the neat P(3HO) and porous patch surfaces
8
9 were modified using optimal electrospun P(3HO) fibres with sizes selected according
10
11 to the highest cell affinity and proliferation observed. P(3HO) fibres were deposited
12
13 on neat and porous P(3HO) films. *In vitro* cell culture work using C2C12 myoblast
14
15 cell line was carried out to assess the final cardiac patches.
16
17

18
19 Finally, as the contractile nature of the cardiac tissue demands readily available high
20
21 oxygen and nutrient concentrations, delivery of angiogenic growth factors from the
22
23 engineered graft is a key factor to encourage the rapid development of the vascular
24
25 network. For this, the vascular endothelial growth factor (VEGF) was incorporated in
26
27 to the patches and VEGF release was studied over 30 days. In addition, for an
28
29 enhanced interaction of the construct with cells, the arginine-glycine-aspartic
30
31 tripeptide sequence (RGD peptide) was immobilized on the patch surface.
32
33
34
35
36
37

38 **2. Materials and Methods**

39 **2.1. P(3HO) production**

40
41 *P. mendocina* was used for the production of poly-3-hydroxyoctanoate, a mcl-PHA.
42
43 The polymer production and extraction and purification were carried out as previously
44
45 described (Rai *et al.*, 2011). The P(3HO) homopolymer was extracted using the
46
47 method involving the dispersion of chloroform and sodium hypochlorite.
48
49
50
51
52
53
54
55
56
57
58
59
60

2.2. P(3HO) characterization

The structural characterization of the obtained polymer was carried out by Fourier transform infrared spectroscopy (FTIR), Gas Chromatography-Mass spectroscopy (GC-MS) and Nuclear magnetic resonance (NMR).

2.2.1. Fourier transform infrared spectroscopy (FTIR)

FTIR analysis was carried out to determine the presence of the PHA functional groups in the sample. A Perkin Elmer series 2000 FTIR spectrometer with a spectral range 4000 to 400 cm^{-1} was used at the Department of Biomaterials and Tissue Engineering, Eastman Dental Institute, University College London, UK. For both, the whole cell analysis and extracted PHA polymer, 2 mg of lyophilised cells or polymer were used.

2.2.2. Gas Chromatography-Mass spectroscopy (GC-MS)

The monomer content of the extracted PHA was identified by GC-MS. Before the analysis, the polymer was methanolysed as previously described (Wang *et al.*, 2006). For this, 15 mg of polymer were added to 1 ml of the esterification solution containing 3 ml of 95–98% H_2SO_4 , 0.29 g of methylbenzoate, and 97 ml of methanol. Then, 1 ml of chloroform was added and the mixture was heated at 100 °C for 4 hr. After the 4 hours, the mixture was cooled and 1 ml of MiliQ water was added and vortexed for phase separation. The lower phase was extracted, dried over anhydrous Na_2SO_4 , neutralized by Na_2CO_3 and filtered (Wang *et al.*, 2006). The analysis was carried out using a Trace2000 GC-MS (Thermo, San Jose, USA) containing a ZB-5MS (Phenomenex, Torrance, CA, USA) column (30 m length, 0.25 mm-internal diameter, and 0.25 μm -film thickness). The sample (1 μL), in chloroform, was injected, with helium (1 mL min^{-1}) as the carrier gas. The injector

1
2
3 temperature was 220 °C and the column temperature was increased from 40 to 320 °C
4
5 at 20 °C min⁻¹ and held at the final temperature for 6 min.
6
7

8 2.2.3. Nuclear magnetic resonance (NMR)

9
10 The extracted PHA monomer structure was confirmed by NMR. The analysis was
11
12 carried out on 30 mg of polymer dissolved in 1 mL of the deuterated chloroform
13
14 (CDCl₃). The ¹H and ¹³C spectra were obtained in a Bruker® AV400 (400 MHz)
15
16 spectrometer at the Chemistry Department, University College London, UK.
17
18
19
20
21
22

23 2.3. Neat and porous P(3HO) cardiac patches fabrication

24
25 The plain and porous films fabrication was carried out by the solvent cast technology.
26
27 For this, 0.5 g of P(3HO) were dissolved in 10 ml of chloroform and poured on 60
28
29 mm diameter glass petri dishes. Porous structures were incorporated by the Solvent
30
31 Casting Particle Leaching (SCPL) technique. In this case, 50 mg of sucrose particles
32
33 between 250 and 300 µm of size, selected using molecular sieves, were added to the
34
35 dissolved polymer before casting. The polymer was dried at the ambient temperature
36
37 (20°C-25°C) for 7 days and then freeze dried for 10 days.
38
39
40
41
42
43
44
45
46
47
48
49
50
51
52
53
54
55
56
57
58
59
60

54 2.4. Neat and porous cardiac patches functionalization with P(3HO) fibrous 55 structures

56
57 The electrospinning technique was used for the fabrication of P(3HO) microfibres.
58
59 For this, the following P(3HO) solutions were produced in acetone: 0.2 wt%, 0.5
60
wt%, 0.6 wt%, 0.7 wt%, 1 wt% and 1.2 wt%. A syringe was loaded with the polymer
solution and pumped by a Harvard® syringe pump through silicone tubing connected

1
2
3 to a nozzle. The conductive steel nozzle was connected to a positive terminal of a
4
5 Glassman Europe® high voltage supply source. The electric potential and the pump
6
7 speed were adjusted for each concentration until a stable jetting was obtained. For the
8
9 optimization of the electrospinning conditions, two sizes of inner diameter nozzles
10
11 (330µm and 660µm) were tested at a range of flow rates (from 30 µl/min to 250
12
13 µl/min). A stable jetting and homogeneous fibres were obtained when the 330 µm
14
15 needle and 30 µl/min flow rate were used and the electric potential was adjusted.
16
17 Higher electric potentials were required with lower polymer concentrations. The
18
19 electric potential used for the 1.2 wt%, 1 wt%, 0.7 wt%, 0.6 wt%, 0.5 wt% and 0.2
20
21 wt% polymer solution were 8.9, 10.9, 11.4, 11.6 13.4 and 13.8, kV respectively. A
22
23 distance of 150 mm between the needle and collector was used in all conditions
24
25 tested. A range of collection times were assessed in each condition (from 1 to 90
26
27 seconds) and one collection time was selected in each case. The fibre collection was
28
29 carried out on plain and porous P(3HO) films and glass slides.
30
31
32
33
34
35
36
37
38

39 **2.5. P(3HO) cardiac patch characterization**

40
41 The physical properties of the material were determined by Dynamic mechanical
42
43 analysis (DMA), Differential scanning calorimetry (DSC) and the surface properties
44
45 were analysed by contact angle analysis, profilometry and scanning electron
46
47 microscopy (SEM).
48

49 *2.5.1. Dynamic mechanical analysis (DMA)*

50
51 The mechanical properties of the polymer were analysed using a Perkin-
52
53 Elmer®dynamic mechanical analyser. The analysis was carried out under static
54
55 conditions on polymer strips of 10 mm length and 4 mm width. The initial load was
56
57
58
59
60

1
2
3 set to 1 mN and then increased to 6000 mN at the rate of 200 mN min⁻¹ and the stress
4
5 and strain were measured. The Young's modulus, tensile strength and elongation at
6
7 break were calculated from the stress vs. strain plot. The experiment was repeated
8
9 after polymer strips were incubated in PBS at 37 °C for two hours.
10

11 12 2.5.2. Differential scanning calorimetry (DSC)

13
14 The thermal properties of the polymer were determined using a Perkin Elmer®Pyris
15
16 Diamond DSC. For the analysis, approximately 8 mg of sample were placed in
17
18 aluminium pans and the samples were cooled down to -57 °C. Then, samples were
19
20 heated, cooled and heated again at a heating rate of 20 °C min⁻¹ from -57 °C to 175
21
22 °C, and the glass transition temperature (T_g), melting temperature (T_m) and
23
24 crystallization temperature (T_c) were determined.
25
26

27 28 2.5.3. Contact angle analysis

29
30 The water contact angle of the fabricated films was analysed on a KSV Cam 200®
31
32 optical contact angle. For this, a Hamilton® syringe was loaded with MiliQ water and
33
34 a drop of water was dispensed on the film. A series of photos were taken every second
35
36 to record the shape of the drop over 20 seconds. The water contact angle was
37
38 measured using a KSVCam® software.
39
40

41 42 2.5.4. Surface roughness analysis

43
44 Surface roughness studies were carried out on a UBM laser scanning
45
46 profilometer. An area of 2 mm x 2 mm (± 500 µm) was scanned by the machine in
47
48 two directions. A graphical representation of the scans and average roughness values
49
50 were recorded.
51
52
53
54
55
56
57
58
59
60

2.5.5. Scanning electron microscopy (SEM)

The surface of the films was examined under a JEOL 5410LV Scanning electron microscope (Hertfordshire, UK). The samples were placed on Agar Scientific® Carbon conducting tabs and then coated with gold-palladium using a Quorum Technologies® Polaron E5000 Sputter Coater (East Sussex, UK) for 2 minutes. The SEM images were taken with an acceleration voltage of 10 kV at 150 mm working distance.

2.5.6. Porosity measurements

The porosity of the films was determined using equation (1).

$$\text{Porosity (\%)} = \frac{V_m - V_p}{V_m} \times 100 = \frac{V_m - (W_p/\rho)}{V_m} \times 100 \quad (1)$$

where V_m is the volume of the plain films, V_p is the volume of the porous film, and $\frac{W_p}{\rho}$, ρ and ρ is the mass and density of the porous film, respectively. Porosity measurements were made in quadruplicates.

2.5.7. Fibre measurements

The size and shape of the fibres obtained by electrospinning was assessed by optical microscopy. Image tool® software was used to measure the size of the fibres. An average of the fibres size was calculated in each condition from the measurement of 30 fibres.

2.6. Cardiomyocyte compatibility studies

2.6.1. Cardiomyocyte viability

1
2
3 *In vitro* biocompatibility studies were performed using freshly isolated Neonatal
4 ventricular rat myocytes (NVRM). P(3HO) patches were cut in to 1 cm² squares,
5
6 placed on a 12 well plate and sterilized using UV light for 30 minutes on each side.
7
8 The NRVMs were seeded on the P(3HO) patches and collagen coated slices, used as
9
10 control, in NRVM medium: 67% Dulbecco's modified Eagle medium (DMEM), 16%
11
12 Medium 199, 10% Horse serum (HS) (Gibco), 4% foetal bovine serum (FBS)
13
14 (Gibco), 2% HEPES (4-(2-hydroxyethyl)-1-piperazineethanesulfonic acid) buffer and
15
16 1% penicillin-streptomycin. Live/dead assay was conducted on day 2 for the NVRM
17
18 cells grown on P(3HO) and collagen. A live/ dead cell cytotoxicity assay was used to
19
20 label the cells. Cells were washed in sterile PBS and 100 µL of 2 µM calcein AM and
21
22 4 µM ethidium homodimer-1 solution was added to each well for 30 min in the dark,
23
24 at room temperature. Following incubation, the samples were mounted in fresh PBS
25
26 and imaged using an inverted Zeiss LSM-780 confocal microscope. Cells were
27
28 counted using the Fiji image processing software (ImageJ). The study was carried out
29
30 in triplicates for each sample.
31
32
33
34
35
36

37 2.6.1.1. Immunofluorescence

38
39 NVRM cells seeded on P(3HO) cardiac patches were washed in phosphate buffered
40
41 saline (PBS), fixed with ice-cold methanol for 5 min and blocked in 1% bovine serum
42
43 albumin (BSA) (subsequently used for all antibody dilutions) for 1 hour. Cells were
44
45 stained with a primary antibody mouse anti- α actinin antibody (1:1000 dilution)
46
47 (sigma) overnight at 4°C and then incubated with a secondary antibody anti-mouse
48
49 Cy3 antibody (1:500 dilution) (Millipore) for 1 hour at room temperature before
50
51 mounting in vectashield (Vectalabs) mounting medium containing DAPI. The cells
52
53 were imaged using an inverted Zeiss LSM-780 confocal microscope.
54
55
56
57
58
59
60

2.6.2. *Cardiomyocyte contraction*

Fresh adult rat beating cardiomyocytes were seeded on a P(3HO) coated cover slip. The cardiomyocytes were superfused at 37°C in modified Krebs-Henseleit solution: NaCl 118.5mM, KCl 5.9mM, NaHCO₃ 25mM, MgSO₄ 1.2mM, NaH₂PO₄ 1.38mM, Glucose 11mM, 1 mM CaCl₂, buffered with 95%O₂/5%CO₂, and delivered at 36-37°C, pH 7.4. For the study, rod shaped cardiomyocytes with regular contraction under electrical stimulation, and no spontaneous contraction without stimulation, were selected. Cells were stimulated with pulses of 50 V for 2 ms with 2 second intervals. Contraction amplitude (% shortening), 'time to peak 90 %' and 'time to relaxation 50 %' were recorded with an IonOptix® video based system. The myocyte contraction was studied at a range of frequencies of electrical pulses of 50 V for a period of 2 ms. Starting from 2 second interval pulses, the intervals were increased to 5 seconds, and then decreased to 2 seconds, 1 second and 0.5 seconds. Following this, the effect of the calcium increment was studied. With a 2 second interval pulse of 2 ms at 50 V, the CaCl₂ concentration of the solution was increased from 1 mM to 2 mM, and then 3 mM and 4 mM. A stabilization period of at least 5 min was allowed in each condition. The contraction studies were also carried out on uncoated cover slips as controls. The contraction experiments were carried out on preparations from 4 animals.

2.7. P(3HO) functionalization with active molecules

2.7.1. *Human vascular endothelial growth factor (VEGF) incorporation within the P(3HO) film*

1
2
3 The VEGF film fabrication was carried out by dissolving 0.5 g of the P(3HO)
4 polymer in 10 ml of chloroform. Then, 2 μl of a 1 $\mu\text{g}/\mu\text{l}$ human VEGF solution in
5 MiliQ water were added into the polymer solution. The resulting solution was
6 vortexed for 5 minutes and cast in 60 mm Petri dishes. Films were dried at 4 $^{\circ}\text{C}$ for 21
7 days.
8
9

10 11 12 13 14 15 *VEGF release kinetics from P(3HO) patches:*

16
17
18 The *in vitro* VEGF release from films was studied for 30 days (Sipahigil *et al.*, 2012).
19 In this experiment 10 mg of films were incubated in Eppendorf tubes containing 1 ml
20 of PBS at 37 $^{\circ}\text{C}$ with constant agitation at 100 rpm. 500 μl of PBS were periodically
21 withdrawn from the tubes and replaced with fresh PBS at the following time points
22 (days): 1, 3, 5, 7, 10, 13, 17, 21, 25 and 30. The amount of VEGF released in the
23 medium was measured using the Invitrogen®VEGF human ELISA kit (R&D
24 Systems, Minneapolis, USA).
25
26
27
28
29
30
31
32

33 34 35 *2.7.2. Arg-Gly-Asp (RGD) peptide patches immobilization*

36
37 The RGD peptide immobilization protocol used in this project was adapted from
38 (Yoon *et al.*, 2003). The immobilization was carried out in two stages. First, the
39 P(3HO) material was aminated and films were cast. Then, the surface immobilization
40 of the RGD peptide was carried out on one side of the aminated solvent cast films.
41 Figure S1 shows the synthetic scheme for the RGD peptide immobilization in PHAs.
42
43
44
45
46
47
48

49 50 51 *Preparation of aminated P(3HO):*

52 In order to attach a terminal amine group to the P(3HO), the carboxylic acid terminal
53 group was activated and reacted with hexaethyleneglycol-diamine. For this, 1 g of
54 P(3HO) was dissolved in 10 ml of methylene chloride. 0.22 mmol of
55
56
57
58
59
60

1
2
3 dicyclohexylcarbodiimide (DCC) and 0.22 mmol of N-hydroxysuccinimide (NHS)
4
5 was added into the polymer solution with stirring. The reaction was stirred for 12 hr at
6
7 the ambient temperature. Insoluble dicyclohexylurea was removed by filtration, and
8
9 the carboxylic group activated polymer was isolated by precipitation in DMSO and
10
11 dried for two days at the ambient temperature. The activated P(3HO) was reacted with
12
13 an excess of hexaethyleneglycol-diamine (75 mg) in 10 ml of methylene chloride for
14
15 12 hr at the ambient temperature with stirring. The aminated P(3HO) was precipitated
16
17 into cold ethanol.
18
19

20
21
22 *Surface immobilization of RGD peptide on aminated P(3HO) films:*
23

24
25 The film casting was carried out by dissolving 0.25 g of aminated P(3HO) with 0.25 g
26
27 of non-aminated P(3HO) (50:50) in 10 ml of methylene chloride. After 5 minutes of
28
29 vortexing, the solution was cast in a glass petridish and dried for 4 days at the ambient
30
31 temperature. Dried films were pre-wetted in 70 % ethanol and washed in distilled
32
33 water. Resulting films were hydrated in PBS for 4 hr. In order to introduce amine
34
35 reactive groups onto the film surface, films were soaked in 20 ml of PBS containing
36
37 100 nM ethyleneglycol-bis-succinimidylsuccinate (EGS) and agitated for 4 hr at the
38
39 ambient temperature. Films were washed with PBS three times and soaked in 20 ml of
40
41 PBS containing 30 nmoles of the RGD peptide. The solution was stirred for 12 hr at
42
43 4 °C. The peptide immobilized films were washed with PBS and distilled water and
44
45 then freeze-dried.
46
47

48
49
50 *Confirmation of the RGD peptide immobilization on P(3HO) films:*
51

52
53 The presence of the RGD peptide on the construct's surface was confirmed by FTIR,
54
55 and contact angle analysis.
56
57
58
59
60

2.8. Cell adhesion and proliferation studies

2.8.1. Sample preparation

P(3HO) film patches were cut in to 1 cm² squares and sterilized under the UV light for 30 minutes each side. P(3HO) films were soaked in supplemented DMEM for 12 hr prior to cell seeding. Cell culture studies were performed in triplicates.

2.8.2. C2C12 cell seeding

C2C12 myoblast cells were grown in DMEM supplemented with 10 % of foetal calf serum, 1% w/v penicillin and 1 % w/v streptomycin solution and grown at 37 °C with 5 % of CO₂. C2C12 myoblast cells in 70 % confluence were used for the cell seeding. Scaffoldex® cell crowns were used to hold the cells on the well's surface. Around 20,000 cells were seeded on the pre-wetted patches in a 24 well plate. As a positive control, cells were seeded in the wells without films. For the negative control, films were incubated in supplemented DMEM without cells. Plates were incubated at 37 °C with 5 % of CO₂ and media was changed every 2 days. Cell proliferation was assessed at 24 hr.

2.8.3. C2C12 MTT assay

The (3-(4,5-Dimethylthiazol-2-yl)-2,5-diphenyltetrazolium bromide) MTT assay was performed on the patches containing the cells at 24 hr according to (Mosmann 1983). For this, 100 µl of a 5 mg/ml MTT solution in distilled water were added to each well at 24 hr and the plates were incubated for two hours at 37 °C with 5% of CO₂. After this, films were transferred to new 24 well tissue culture plates and 500 µl of DMSO was added. After a 5 minute incubation, 100 µl of the resulting solution were transferred to 96 well plates and the absorbance at 540 nm was measured on a

1
2
3 Thermomax® microtitre plate reader. The absorbance of the samples were normalised
4
5 with respect to the positive control. The difference in the surface areas of the tissue
6
7 culture plate wells and the films were considered for the calculation of the % cell
8
9 viability on the films.
10

11 12 2.8.4. C2C12 myoblast SEM 13

14
15 At 24 hr, patches containing the cells were visualized using SEM. To this end, cells
16
17 were fixed in 0.1 M cacodylate buffer containing 3% glutaraldehyde for 12 hr at 4 °C
18
19 and dehydrated in a series of ethanol solutions (50 %, 70 %, 90 % and 100 %) for four
20
21 times, incubating 10 minutes in each solution. Samples were air dried, coated and
22
23 examined under the SEM.
24
25
26
27
28

29 2.9. Data analysis 30

31
32 Data are reported as mean \pm STDEV. Statistical significance was assessed using
33
34 ANOVA with the Newman-Keuls' test. Differences were considered statistically
35
36 significant when $P < 0.05$.
37
38
39
40
41

42 3. Results 43

44 3.1. P(3HO) patch production and structural characterization 45

46
47 The polymer was produced using *Pseudomonas mendocina* and purified as previously
48
49 described (Rai *et al.*, 2011). Structural characterization of the resulting polymer was
50
51 carried out by FTIR, GC-MS and NMR. The results obtained confirmed the presence
52
53 of the P(3HO) homopolymer.
54
55
56
57
58
59
60

3.2. P(3HO) patch production and physical characterization

3.2.1. Mechanical properties

P(3HO) patches (5 wt%) were fabricated by solvent casting and mechanical characterization was carried out by dynamic mechanical analysis. The Young's modulus of the resulting patch was 3.7 ± 0.3 MPa. The % elongation at break and the tensile strength, obtained at the maximum elongation, before the material is fractured was 299 ± 3 % and 3.4 ± 0.2 MPa, respectively. In a preliminary study, in order to understand the possible mechanical response of the patches to the body environment, mechanical properties were measured after incubating the samples in PBS buffer at 37°C for two hours. The Young's modulus, % elongation at break and the tensile strength were measured to be 1.5 ± 0.4 MPa, 699.3 ± 113 % and 10.1 ± 1.4 MPa, respectively. Hence, at body temperature, the P(3HO) patch is less stiff, closer that of the myocardial stiffness of 0.02-0.5 MPa, has higher elongation at break and higher tensile strength, all features showing a further improvement over the measurements made at room temperature with a dry sample.

Controlled porosity in biomaterials is a key factor when they are used as a physical support for cell adhesion and growth (Lebourg *et al.*, 2008). Porous P(3HO) patches were created by the particle leaching method and the effect of porosity on the mechanical properties was studied. For this, 0.5% sucrose with controlled particle size ranging from 250 to 300 μm was used as the porogen. Resulting patches showed a percentage porosity of 28 ± 5 %. Mechanical properties of the porous patches were measured. The obtained Young's modulus, tensile strength and elongation at break were 0.41 ± 0.03 MPa, 0.7 ± 0.1 MPa and 447 ± 5 %, respectively. As described above, the Young's modulus of the human myocardium is 0.02-0.5 MPa, hence, the stiffness

1
2
3 of the resulting P(3HO) porous patches was exactly in the range of the human
4 myocardial structures, crucial to allow a synchronic beating of a myocardial
5 engineered tissue.
6
7
8
9

10 3.2.2. *Thermal properties*

11
12 The thermal properties of the material were determined by differential scanning
13 calorimetry analysis. The thermograms showed the presence of two peaks
14 corresponding to the melting temperature and glass transition temperature. The
15 melting temperature obtained was 43.7 ± 4.1 °C and the glass transition temperature
16 was -32.9 ± 3.8 °C. The low melting temperature obtained together with a glass
17 transition temperature below the ambient temperature indicates the elastomeric nature
18 of the obtained P(3HO) polymer.
19
20
21
22
23
24
25
26
27
28
29

30 3.3. Functionalization of P(3HO) patches with fibres

31 3.3.1. *P(3HO) fibre production*

32
33 In order to mimic the fibrillar structure of the extracellular matrix which provides
34 essential guidance for cell organization, survival and function, P(3HO) fibres were
35 created by electrospinning. Electrospinning is a process based on the production of
36 fibres by the application of a high voltage source to a polymer dissolved in a suitable
37 solvent. For the optimization of the electrospinning conditions, a range of P(3HO)
38 solutions were created in acetone (0.2 wt%, 0.5 wt%, 0.6 wt%, 0.7 wt%, 1 wt% and
39 1.2 wt%). The size of the fibres obtained in each condition was measured by optical
40 microscopy and the results are shown in Table 1. It was observed that the fibre
41 diameters decreased with decreasing P(3HO) concentration and particles rather than
42 fibres were obtained with the lowest concentration. In the case of 0.5 wt% P(3HO)
43
44
45
46
47
48
49
50
51
52
53
54
55
56
57
58
59
60

1
2
3 solution, a transition between fibre formation and particle formation occurred, hence,
4
5 both fibres and particles were obtained.
6

7 8 **TABLE 1**

9
10 In order to determine the most suitable fibre or particle size to be used for the design
11 of cardiac patches, fibres or particles were collected from the 1.2 wt%, 1 wt%,
12 0.7 wt%, 0.6 wt%, 0.5 wt% and 0.2 wt% polymer solution on glass slides for 10
13 minutes to ensure that the full surface of the slides were covered. In the following
14 experiments cell proliferation on the P(3HO) fibres was assessed with the C2C12
15 myoblast cell line. Cells were seeded on the glass slides coated with different sizes of
16 P(3HO) fibres or particles. Cell adhesion and proliferation were determined after
17 24 hrs using the MTT colorimetric assay. Figure 1 shows the results obtained. Our
18 results showed that an increment in fibre diameter resulted in a higher % cell
19 proliferation, achieving the highest value of 196.8 ± 16.0 with 750 nm fibres. Also,
20 cells showed preference for fibrous structures as compared to particle structures.
21
22
23
24
25
26
27
28
29
30
31
32
33
34

35 **FIGURE 1**

36
37 Several studies have shown that fibrous matrices, which allow cell infiltration into
38 their porous structure, are attractive substrates as tissue engineering scaffolds (Lee *et*
39 *al.*, 2011, Krupnick *et al.*, 2001). Pores in an electrospun fibrous structure are formed
40 by nonaligned fibres and the size and shape of those pores will be directly related to
41 the fibre concentration. In order to find the optimal concentration of fibres that will
42 allow cell infiltration, in the next experiment, the collection times for the 750 nm
43 fibres on glass slides were varied from 1 to 90 seconds and the fibre concentration
44 was evaluated by optical microscopy. The selected collection time was 30 seconds, in
45 which the fibres covered the entire surface, leaving some gaps for the cells to
46 infiltrate.
47
48
49
50
51
52
53
54
55
56
57
58
59
60

3.4. P(3HO) surface characterization studies

The surface structure of the neat P(3HO) and porous patches with or without fibrous structures was characterized in terms of wettability, roughness and SEM. The surface wettability of the patches was studied with a contact angle meter. The water contact angle on the neat P(3HO) patches was $101.1 \pm 0.8^\circ$, indicating a hydrophobic surface. The obtained water contact angle for the porous patches was $104.9 \pm 6.0^\circ$. The water contact angles measured for the plain and porous patches functionalized with fibres were 110.2 ± 3.7 for neat P(3HO) patches containing 750 nm fibres and 99.8 ± 1.9 for porous patches containing 750 nm fibres. Surprisingly, an increment in the surface hydrophobicity was observed when neat patches were functionalized with fibres and a decrease in the surface hydrophobicity was observed when porous patches were functionalized with fibres.

The surface roughness properties of the different patches was studied. Results indicate that the average surface roughness of the P(3HO) neat and porous patches was $0.17 \mu\text{m}$ and $0.9 \pm 0.2 \mu\text{m}$, respectively. The average surface roughness of the patches functionalized with fibres was $0.90 \pm 0.01 \mu\text{m}$ for neat patches and $1.1 \pm 0.1 \mu\text{m}$ for porous patches. As expected, an increment in the surface roughness was observed when patches were functionalized with fibrous structures, achieving the maximum roughness when porous and fibrous structures were combined.

Finally, the surface morphology and microstructure of the P(3HO) neat and porous patches was visualized using scanning electron microscopy.

3.4.1. *In vitro* cell proliferation studies

1
2
3 As the structure of the P(3HO) fibres was intended for cardiac tissue engineering, its
4 suitability was initially evaluated *in vitro* using C2C12, a myoblast cell line. Cells
5 were seeded on the cardiac patches and the % cell proliferation was assessed at 24 hrs
6 with the MTT colorimetric assay. Cell proliferation results for the different patches
7 were compared. The results showed that the % cell proliferation increased 2.5 fold
8 when porous structures were incorporated on the P(3HO) patches (Figure 2).
9 Additionally, a significant increment in the % cell proliferation was obtained when
10 fibre structures were incorporated on the surface of the neat P(3HO) and porous
11 patches. Similar values for cell proliferation were observed with the porous and neat
12 patches modified with fibres, suggesting that both structures contribute in a similar
13 way to cell proliferation. Finally, P(3HO) porous patches containing the P(3HO)
14 fibrous structures showed the highest cell proliferation rate and hence this was the
15 best matrix for cell adhesion and proliferation.
16
17
18
19
20
21
22
23
24
25
26
27
28
29
30
31

32 **FIGURE 2**

33
34
35 SEM analysis was carried out to visualize the C2C12 myoblast cell line on the neat
36 and porous P(3HO) patches with and without fibres. Figure 3 shows typical SEM
37 images observed for samples after 24 hr of cell growth. These results showed that at
38 24 hr the surface of the porous cardiac patches is covered with cells and that cells
39 grew inside the pores, almost covering the pore structures. For P(3HO) patches
40 functionalized with fibrous structures, it is possible to observe cells growing on top of
41 the first cell layer.
42
43
44
45
46
47
48
49
50

51 **FIGURE 3**

52 **3.5. Cardiomyocyte cytocompatibility studies**

3.5.1. Cardiomyocyte viability on P(3HO) patches

The biocompatibility of the P(3HO) polymer was further assessed by comparing the number of live/dead NVRM cells on both P(3HO) patches and collagen coated wells. The ratios of live/dead NVRM cells are illustrated in Figure 4. These results show similar viability on both P(3HO) polymer and collagen, showing that P(3HO) is equally biocompatible towards cardiomyocytes as compared to collagen, the current gold standard for cardiac tissue engineering. Figure 5 shows confocal microscopy images of the NVRM cells labeled with ethidium homodimer-1 growing on P(3HO) polymer and collagen, and anti α -actinin and DAPI immunofluorescent imaging, showing NVRM cells growing on P(3HO) patches and forming well-formed sarcomeres, confirming high biocompatibility of the patches.

FIGURE 4

FIGURE 5

3.5.2. Cardiomyocytes' contraction on P(3HO) patches

The effect of the P(3HO) polymer on the contraction of the cardiomyocytes was studied. Fresh isolated adult rat cardiomyocytes were seeded on P(3HO) coated cover slips and superfused in a Krebs-Henseleit solution at 37°C and bubbled with 95% O₂, 5% CO₂. Cover slips without coating were used as controls. For the study, rod shaped cardiomyocytes with regular stimulated contractions but no spontaneous contraction without stimulation were selected. Cells were stimulated with pulses of 50 V for a period of 2ms with 2 second intervals. The contraction amplitude (% shortening), time to peak 90% and time to relaxation 50% were recorded with a video and analyzed with the Inoptix program.

1
2
3 The effect on cardiomyocyte contraction with P(3HO) polymer as the substrate, when
4 cells were stimulated at a range of electrical pulses and calcium concentrations, was
5 studied. Figure 6A shows the effect on cardiomyocyte contraction (% shortening) for
6 both polymer and control when the intervals of electrical pulses were varied for 2, 5,
7 2, 1 and 0.5 second interval. No differences were observed in % shortening between
8 polymer and control. A significant reduction in % shortening was observed in the
9 control when the intervals of electrical pulses decreased from 5 to 2, 1 and 0.5
10 seconds but not in the polymer. These results indicate the capacity of the
11 cardiomyocytes to maintain a sustained contraction capacity when P(3HO) was used
12 as the substrate, an essential and excellent property for Cardiac Tissue Engineering.
13
14
15
16
17
18
19
20
21
22
23
24
25

26 The calcium concentration in the Krebs-Henseleit solution was increased from 1 to 2,
27 3 and 4 mM when P(3HO) or glass coverslips were used as the base matrix. Figure
28 6(B) shows the effect on cardiomyocyte contraction (% shortening) at 1, 2, 3 and 4
29 mM calcium for both polymer and control. There was a tendency for contraction to
30 increase with increasing calcium, but no significant difference was observed between
31 the control and P(3HO) at any concentration.
32
33
34
35
36
37
38
39

40 **FIGURE 6**

41
42
43 Table 2(A) and 2(B) show 'time to peak 90%' and time to 'relaxation 50%' for
44 control and P(3HO) polymer at different interval of pulses and different calcium
45 concentrations, respectively. Contraction amplitude (% shortening) decreased
46 significantly with reduced interval, but there was no significant difference between
47 behaviour on polymer vs. control. Results showed no differences in 'time to peak
48 90%' and time to 'relaxation 50%' between polymer and control.
49
50
51
52
53
54
55
56

57 **TABLE 2**

3.6. P(3HO) functionalization with active molecules

3.6.1. RGD immobilization

The cell-polymer and cell-cell interactions play a key role in controlling cell adhesion, proliferation, migration and differentiation. Several reports show the role of the RGD peptide in controlling these interactions (Yoon *et al.*, 2003, Hersel *et al.*, 2003, Rezanian and Healy 2008). In order to improve the properties of the P(3HO) cardiac patches, RGD peptides were immobilized onto the surface of the patch. The RGD peptide immobilization protocol used in this work was adapted from (Yoon *et al.*, 2003), where RGD motifs were immobilized on PLGA. Firstly, the carboxylic acid terminal group of P(3HO) was aminated by reacting the polymer with hexaethyleneglycol-diamine. FTIR was carried out to confirm that the amination had occurred. The FTIR spectrum obtained from the modified P(3HO) patch was compared with the neat P(3HO) polymer patch. Results show the presence of a band at 3400 cm^{-1} , which corresponds to the N-H bond. Additionally, a band was observed at 1000 cm^{-1} confirming the presence of a C-N bond. These absorbance peaks were missing in the neat polymer patch. This result confirmed that the P(3HO) patch had been successfully aminated. The aminated P(3HO) polymer was blended with equal amounts of P(3HO) (50:50) and patches were fabricated by the solvent casting technique. The resultant patches were modified with RGD tripeptides on one side of the structure. In order to verify the presence of RGD motifs covalently linked to the membrane, FTIR was carried out. The FTIR spectra obtained from the RGD immobilized P(3HO) film was compared with the as synthesized P(3HO) film. Results showed the presence of a strong band at 1287 cm^{-1} corresponding to the C-N bonds present on the RGD-P(3HO) polymer. Also, other bands were observed at 825 cm^{-1} , 1047 cm^{-1} and 1226 cm^{-1} due to the bend of the N-H bond and the stretch of C-

1
2
3 O and C-O-C bonds from the poly(ethylene glycol) (PEG) group linked to the
4 structure, respectively. Finally, as expected, the band observed at 3400 cm^{-1}
5
6
7 corresponding to the $-\text{NH}_2$ functional group was not observed in this case. This is due
8
9
10 to the fact that this terminal amine group would have reacted with the RGD sequence
11
12 and hence the new terminal group is the carboxylic group from the RGD peptide.

13
14 Previously various groups have shown the relation between RGD immobilization and
15
16 surface wettability. It was observed that the incorporation of RGD structures on the
17
18 surface of the polymer has a direct effect in decreasing the hydrophobicity of the
19
20 structure. In order to confirm the presence of RGD motifs linked to the P(3HO)
21
22 cardiac patches, the surface wettability of the cardiac patches was analysed. The water
23
24 contact angle obtained for the P(3HO)-RGD film was $93.4\pm 0.1^\circ$. P(3HO) water
25
26 contact angle was $101.1\pm 0.8^\circ$. Our results show a significant decrease in the water
27
28 contact angle, which indirectly confirms the presence of the RGD immobilized
29
30 peptide.
31
32

33
34 As described previously, mechanical properties of the cardiac patch play an essential
35
36 role in the patch function supporting the heart during regeneration. In order to study
37
38 the possible influence of the P(3HO) modification on the patch mechanical properties,
39
40 dynamic mechanical analysis was carried out on P(3HO)-RGD cardiac patches. The
41
42 Young's modulus of the RGD modified film was 3.9 MPa. The P(3HO) neat patches'
43
44 Young's modulus was 3.7 ± 0.3 MPa, hence no differences were observed in terms of
45
46 Young's modulus after the RGD modification. The tensile strength for P(3HO)-
47
48 RGD was 0.7 MPa and elongation at break 426.5%. The tensile strength and
49
50 elongation at break for P(3HO) was 3.4 ± 0.2 MPa and 299 ± 3 %, respectively. These
51
52 results show a decrease by 19% in tensile strength and an increase by 42% in
53
54 elongation at break after the RGD modification. In order to visualize the surface of
55
56
57
58
59
60

1
2
3 the modified cardiac patches, SEM was carried out. Figure S2 shows the SEM images
4 of P(3HO)-RGD cardiac patches. These pictures revealed that the incorporation of
5 RGD peptide structures changed the surface morphology of the patch by introducing a
6 rough topography on the surface.
7
8
9
10

11 12 13 *3.6.2 VEGF incorporation in P(3HO) patches*

14
15 As vascularisation and angiogenesis are key factors in cardiac tissue engineering,
16 VEGF was incorporated into the P(3HO) patches. The mechanical properties of the
17 resulting cardiac patches were measured. The Young's modulus obtained for the
18 VEGF modified film was 6.8 MPa, the tensile strength was 0.6 MPa and the
19 elongation at break was 449.3%. The tensile strength and elongation at break for
20 P(3HO) was 3.4 ± 0.2 MPa and 299 ± 3 %, respectively. These results show a decrease
21 in tensile strength by 17% and an increase by 50% in elongation at break after the
22 VEGF incorporation. The surface of the VEGF modified cardiac patches was
23 analysed by water contact angle measurement and SEM. The water contact angle of
24 the P(3HO) cardiac patches containing VEGF factor incorporated was $102.5 \pm 1.4^\circ$
25 and that of neat P(3HO) was $101.1 \pm 0.8^\circ$. These results show no differences in the
26 surface wettability with VEGF incorporation.
27
28
29
30
31
32
33
34
35
36
37
38
39
40
41
42

43 *3.6.3. Cell proliferation on RGD and VEGF patches*

44
45 The effect of P(3HO)-RGD immobilized cardiac patches and P(3HO)-VEGF on cell
46 proliferation as compared to the neat polymer patch was studied. C2C12 myoblast
47 cells were seeded on P(3HO) modified cardiac patches and cell proliferation was
48 measured by the MTT colorimetric assay. Figure 7 shows the % cell proliferation on
49 P(3HO), P(3HO)-VEGF, P(3HO)-RGD and P(3HO)-VEGF+RGD cardiac patches
50 when proliferation observed on tissue culture plastic was considered to be 100%. The
51
52
53
54
55
56
57
58
59
60

1
2
3 % cell proliferation on P(3HO) patches was 21.11 ± 5.29 %. A significant increase in
4
5 cell proliferation was observed when VEGF and RGD were incorporated into the
6
7 P(3HO) cardiac patches. However, a higher cell proliferation was achieved with
8
9 VEGF. A synergistic effect was observed when both VEGF and RGD were
10
11 incorporated together, showing a highly significant effect on cell proliferation.
12
13

14 15 **FIGURE 7**

16 17 18 *3.6.4. VEGF release*

19
20 The cumulative *in vitro* release of VEGF from P(3HO) cardiac patches was studied
21
22 over 30 days. The amount of VEGF released in the medium was measured using the
23
24 Invitrogen® VEGF human ELISA kit. The release profile is shown in Figure S3. Our
25
26 results showed a biphasic VEGF release for P(3HO) cardiac patches with an initial
27
28 burst release followed by a period of sustained release.
29
30
31
32
33
34

35 36 **4. Discussion**

37
38 Medium chain length PHAs, with a typical monomer chain length from 6-16 carbon
39
40 atoms, are polymers produced by bacteria. Mcl-PHAs are of great interest because
41
42 according to the number of carbons in the side chain, the physical properties of these
43
44 biodegradable polymers can be varied, allowing the production of tailor made
45
46 functional materials. Previous reports have shown that mcl-PHAs are flexible
47
48 elastomeric polymers, with low crystallinity, low glass transition temperature, low
49
50 tensile strength, and high elongation to break (Zinn *et al.*, 2001). In this work we
51
52 studied poly(3-hydroxyoctanoate), a mcl-PHA, as a potential novel functional
53
54
55
56
57
58
59
60

1
2
3 material for cardiac tissue engineering. P(3HO) was known to be produced as a
4
5 homopolymer by *P. mendocina*, as previously described (Rai *et al.*, 2011).
6
7

8 **4.1. P(3HO) engineered patches**

9

10
11 Engineering biomaterials to promote cell adhesion and direct cellular behavior is
12
13 crucial for the development of materials capable of restoring tissue function. Several
14
15 reports have proven that cells are sensitive to the physical and chemical environment
16
17 which determines cell specific migration, proliferation, differentiation and production
18
19 of proteins which in turn influences tissue organization and regeneration (Shin *et al.*,
20
21 2004). Several studies on creating beating engineered synthetic patches have been
22
23 reported recently showing that the stiffness of the scaffold impeded the contractions
24
25 (Shin *et al.*, 2004). Additionally, due to the myocardial tissue cyclic and constant
26
27 beating, a plastic deformation and failure is expected when thermoplastic polymers
28
29 such as polyglycolic acid (PGA), polylactic acid (PLA) and poly(ϵ -caprolactone)
30
31 (PCL) and their copolymers are exposed to long term cyclic strain. Table 3 shows the
32
33 mechanical properties of some of the materials that have been explored for
34
35 myocardial tissue engineering. These data show that most natural materials are
36
37 weaker than myocardial structures in contrast to synthetic materials, which are much
38
39 stiffer than the human myocardium.
40
41
42
43
44

45 **TABLE 3**

46
47
48 Although most synthetic materials do not have the desirable mechanical properties for
49
50 cardiac tissue engineering applications, some of these polymers can be tuned by
51
52 introducing different structures in the polymer backbone. Among the different
53
54 synthetic polymers, polyurethanes seem to be the most versatile due to their large
55
56 number of building blocks (macrodiols, diisocyanates and chain extenders) that allow
57
58
59
60

1
2
3 the introduction of peptide sequences and several types of biomolecules in the
4
5 polymeric chain (Silvestri *et al.*, 2014). However, different polyurethanes have shown
6
7 various problems such as hydrolysis, oxidation, environmental stress cracking,
8
9 thrombosis and calcification *in vivo* (Guan *et al.*, 2005, Ma *et al.*, 2012, Santerre *et*
10
11 *al.*, 2005). Hence, several groups have worked towards improving the polyurethane
12
13 properties via incorporation of peptide sequences and biomolecules to the
14
15 polyurethanes chain to achieve the desirable properties active tissue engineering.
16
17 Guan *et al.*, 2008 and Silverstri, *et al.*, 2013 have focused on the enhancement of the
18
19 polyurethane elasticity, strength and biodegradable properties. A biodegradable
20
21 polyurethane containing an elastase-sensitive peptide sequence was developed.
22
23 Although the mechanical, biological and biodegradation properties were improved *in*
24
25 *vitro*, *in vivo* experiments need to be carried out to test the capability of the patches to
26
27 recruit cardiac cells and restore mechanical and biological functions of the infarcted
28
29 ventricle.
30
31
32
33
34

35 In this work we have looked in to the development of cardiac patches using a
36
37 relatively unexplored family of polymers, polyhydroxyalkanoates, more specifically,
38
39 P(3HO). In the first part of this work, P(3HO) based plain and porous patches were
40
41 created by the solvent casting and solvent casting particle leaching, respectively.
42
43 Porosity was incorporated in order to allow cell ingrowth. As P(3HO) is a
44
45 biodegradable material, it is anticipated that the biomaterial structure will reabsorb
46
47 leaving behind new tissue. The average diameter of the pores was 250-300 μm , which
48
49 is close to the size of adult human myocytes. It is important to mention that although
50
51 porous structures provide more surface for cell residence, the number of porous
52
53 structures that can be created are limited by the desired mechanical properties of the
54
55 biomaterial. Materials with high porosities displayed diminished mechanical
56
57
58
59
60

1
2
3 properties (Golstein *et al.*, 1995). As one of the main requirements for a biomaterial in
4
5 cardiac tissue engineering is to support the high mechanical demands of the organ
6
7 during regeneration, the porogen concentration, which would determine the porosity
8
9 in the patch, was chosen to allow some cell ingrowth without substantial deterioration
10
11 of the mechanical properties. For this, P(3HO) porous patches were made using 0.5
12
13 wt% polymer solution. The resulting patches were fully characterized and assessed
14
15 for cardiac tissue engineering applications. The mechanical properties of the material
16
17 plays a crucial role in supporting the injured organ during regeneration. The P(3HO)
18
19 patches' mechanical properties were measured before and after the samples were
20
21 incubated in PBS at 37°C. As myocardial stiffness is considered to be an essential
22
23 myocardial property, especially during the diastole, stiffness was quantified by
24
25 examining the relationship between stress and strain (Nagueh *et al.*, 2004). The
26
27 Young's modulus of the P(3HO) neat film before and after incubation in PBS at 37°C
28
29 was 3.7±0.3 MPa and 1.4±0.4 MPa, respectively. Hence, although a decrease in the
30
31 P(3HO)'s stiffness was observed after incubating the samples in PBS buffer at 37°C,
32
33 the obtained value was in fact closer to the Young's modulus value of the human
34
35 myocardium (0.02-0.5 MPa), an excellent improvement. In addition, the Young's
36
37 modulus value of the porous film was 0.41±0.03 MPa, which is exactly within the
38
39 range of the stiffness of the human myocardium. As the lower value of myocardial
40
41 stiffness is 0.02 MPa, it is possible to further increase the number of porous structures
42
43 and decrease the stiffness of the construct even further. However, as after a
44
45 myocardial infarction there is an increasing load on the heart wall we hypothesized
46
47 that among the range of cardiac patches, the one with a higher stiffness is best suited
48
49 for myocardial support (Sutton and Shape 2000). The ability to resist failure under
50
51 tensile stress is one of the most important properties of materials used in structural
52
53
54
55
56
57
58
59
60

1
2
3 applications. The tensile strength obtained for P(3HO) patches before and after
4
5 incubation in PBS at 37°C and porous patches were 3.4±0.2 MPa, 10.1±0.4 MPa and
6
7 0.7±0.2 MPa, respectively. Although these values are higher than myocardial
8
9 structures (human myocardium tensile strength 3-15 kPa), a higher tensile strength
10
11 might have a positive effect as after a myocardial infarction, the abrupt loss of
12
13 myocardium triggers a ventricular remodeling that includes dilatation, hypertrophy,
14
15 and the formation of a collagen scar that increases the load on the infarcted region.
16
17 Furthermore, it has been described that negative ventricular remodeling continues for
18
19 weeks or months until the distending forces on the cardiac tissue are counterbalanced
20
21 by the tensile strength of the collagen scar, hence, a higher tensile strength could have
22
23 a positive effect after a myocardial infarction (Sutton and Sharpe 2000) Finally, the
24
25 percentage elongation at break of neat P(3HO) patches before and after incubation in
26
27 PBS at 37°C and porous patches was 299±3 %, 699±113 % and 447±5 %,
28
29 respectively. These values show that neat P(3HO) polymer patches have an
30
31 elongation at break in the range of myocardial structures and this value is somewhat
32
33 higher for both the neat P(3HO) patch incubated in PBS at 37°C and porous patches
34
35 (human myocardial elongation at break is between 100-300 %). This further confirms
36
37 the suitability of P(3HO) based cardiac patches for myocardial repair and
38
39 regeneration.
40
41
42
43
44
45

46 In order to define the processability of the material, the thermal properties of the
47
48 polymer were determined by differential scanning calorimetric analysis. Thermal
49
50 analyses of P(3HO) showed two peaks corresponding to the glass transition
51
52 temperature and melting temperature observed at -32.9±3.8 °C and 43.7±4.1 °C during
53
54 the first heat scan, respectively. A glass transition temperature below ambient
55
56 temperature and the low melting temperature, which reflects the low crystallinity of
57
58
59
60

1
2
3 the polymer imparts an elastomeric behavior to the material. Although the melting
4
5 temperature of P(3HO) is quite close to the human body temperature, the mechanical
6
7 testing carried out in PBS, at 37°C, described above, have proven that the mechanical
8
9 properties of the P(3HO) patches remain suitable for cardiac tissue engineering, i.e.,
10
11 the Young's modulus, tensile strength and elongation at break values remain similar
12
13
14 to that of the myocardium.
15

16 17 **4.2. Surface functionalization**

18
19 The extracellular matrix provides not only structural support to the cells but also
20
21 regulatory cues for cells assembling into tissues, for growth and communication. As a
22
23 result, one of the main goals in tissue engineering is to develop a tailored *in vitro*
24
25 environment that mimics the intricate and organized mesh of native extracellular
26
27 matrix. As the extracellular matrix is mainly composed of collagen fibrils, the
28
29 structure and topography of the fibres were recreated by electrospinning.
30
31 Electrospinning is a versatile technique which allows the fabrication of nano and
32
33 micro scale fibres or particles which mimic the extracellular matrix architecture.
34
35 Different P(3HO) concentrations ranging from 0.2 wt% to 1.2 wt% were used to
36
37 create electrospun fibres. The results obtained showed an increment in the fibre
38
39 diameter from 340 nm to 750 nm when the polymer concentration was increased from
40
41 0.6 wt% to 1.2 wt% (Table 1). These results were in agreement with Boland *et al.*,
42
43 (2001) who showed a direct relation between polymer concentration and electrospun
44
45 fibre diameter (Boland *et al.*, 2001). When the P(3HO) concentration was 0.5 wt%,
46
47 both fibres and particles were obtained. Only particles were obtained with 0.2 wt%
48
49 polymer solution.
50
51
52
53
54
55
56
57
58
59
60

1
2
3 In order to find out the most suitable matrix for cells to grow, glass slides were coated
4 with the different fibre sizes obtained. C2C12 myoblast cells were seeded on the
5 electrospun coated slides. The results obtained showed that the fibre diameter has a
6 direct effect on cell adhesion and proliferation, with an increment in cell density with
7 fibre size. The adhesion of cells to the extracellular matrix is mediated through focal
8 adhesions, large protein complexes organized at the basal surface of cells, which
9 connects the cytoskeleton of the cell to the matrix. Previous studies have shown that
10 differences in fibre diameter result in highly significant differences in focal adhesion
11 formation and cell proliferation (Hsia *et al.*, 2011). In contrast to our results, Chen *et*
12 *al.*, (2007) observed an increment in fibroblast adhesion as a function of decreasing
13 electrospun polycaprolactone fibre diameter from 1051 to 428 nm (Chen *et al.*, 2007).
14 We hypothesize that differences observed in these studies may be related to
15 differences in cell size, however, further studies should be carried out to elucidate
16 how the fibre size affects cell adhesion and proliferation.
17
18
19
20
21
22
23
24
25
26
27
28
29
30
31
32
33
34

35 It is important to mention that fibre diameter also has a crucial role in controlling the
36 pore diameter of the networks. It has been proven that increasing fibre diameter
37 results in an increase in mean pore radius and hence cellular ingrowth. (Eichhorn and
38 Sampson 2005). Previous findings have shown that nanofibre structures impede cell
39 migration into the scaffolds as they act as a sieve, keeping cells on the surface of the
40 scaffold (Balguid *et al.*, 2009). In order to allow cell migration into the interior of the
41 electrospun fibres and porous structures, different collection times were assessed. The
42 selected collection time was 30 seconds, the one in which the fibres have covered the
43 full area leaving gaps for the cells to infiltrate. Although some pores were smaller
44 than myocardial cells, they should not impede cell migration as the fibres are lying
45
46
47
48
49
50
51
52
53
54
55
56
57
58
59
60

loosely upon each other and cells perform amoeboid movements to migrate through the pores by pushing fibres (Laurencin *et al.*, 2002).

4.3. Surface characterization

The surface of the biomaterials plays a significant role in determining the outcome of the biological system and biomaterial interaction (Flemming *et al.*, 1999). The hydrophobicity of a biomaterial surface is directly related to cell adhesion. The cell adhesion to a surface occurs by adhesion receptors present in the cell that binds to proteins adsorbed on the surface and the conformation of these proteins depends on the surface wettability (Lee *et al.*, 2003). It has been described that the water contact angle of hydrophobic surfaces is higher or equal to 90° (Li 2011). The P(3HO) patches' water contact angle was $101.1 \pm 0.8^\circ$ for neat polymer patches and $104.9 \pm 6.0^\circ$ for porous patches. For the patches modified with fibres the water contact angle measured was 110.2 ± 3.7 for neat P(3HO) patches containing 750 nm fibres and 99.8 ± 1.9 for porous patches containing 750 nm fibres. An increment in the surface hydrophobicity was observed when neat patches were functionalized with fibres and a decrease in the surface hydrophobicity was observed when porous patches were functionalized with fibres. It has been described that the wettability depends on the type of material as well as the surface treatment of the material (Lu and Chung 1998). Our results show that the P(3HO) patches' surface is hydrophobic, however, the value is not much higher than the upper limit of 90°, known for hydrophilic surfaces. In general, hydrophilic surfaces display better affinity for cells as compared to hydrophobic surfaces (Lampin *et al.*, 1997), however, our biocompatibility test results confirmed the excellent cell attachment and proliferation on the P(3HO) patches, comparable to that of collagen. This indicates the possible adherence of media

1
2
3 proteins on the surface of the P(3HO) which in turn results in excellent cell
4
5 attachment and proliferation properties.
6
7

8
9
10 With regard to roughness of the surface affecting the growth of different kinds of
11
12 cells, most researchers have shown that increased surface roughness has a positive
13
14 effect on cell adhesion (Richert *et al.*, 2008). The surface roughness of the film was
15
16 measured using the white light interferometry technique. The surface roughness of the
17
18 cardiac patches was $0.90 \pm 0.01 \mu\text{m}$ for neat patches with 750 nm fibres and 1.1 ± 0.1
19
20 μm for porous patches with 750 nm fibres. The surface roughness of the neat and
21
22 porous P(3HO) patches was $0.2 \mu\text{m}$ and $0.9 \pm 0.2 \mu\text{m}$. These results showed that the
23
24 incorporation of porous and fibrous structures increases the surface roughness by
25
26 approximately 5 fold and by 6.5 fold, respectively, a positive feature for a material to
27
28 be used for the development of a cardiac patch.
29
30

31
32 SEM analysis and surface roughness studies revealed that the P(3HO) neat polymer
33
34 patches present a smooth surface. The visualization of the fibres by SEM was not
35
36 possible due to the high temperature sensitivity of the P(3HO) fibrous structures
37
38 which melted under the SEM focused beam of high-energy electrons.
39
40

41
42 Several groups show the influence of surface wettability and roughness in the cell-
43
44 biomaterial interaction, however, no general principles that can help in the prediction
45
46 of cellular behavior by the combination of these parameters are known. Therefore,
47
48 cell adhesion and proliferation were assessed. Myoblast (C2C12) cell proliferation was
49
50 analyzed and compared on neat P(3HO) patches, porous patches, neat P(3HO)
51
52 polymer cardiac patches with 750 nm diameter fibres and porous cardiac patches with
53
54 750 nm diameter fibres on their surface. The proliferation observed on these patches
55
56 were $21.1 \pm 1.9 \%$, $53.8 \pm 3.1 \%$, $41.6 \pm 2.4 \%$ and $109.2 \pm 1.5 \%$, respectively, when
57
58
59
60

1
2
3 proliferation observed in tissue culture plates was considered to be 100 %. Results
4
5 showed that both porous and fibrous structures increased the % cell proliferation due
6
7 to their higher surface area-to-volume ratio as well as their topographical features that
8
9 can enhance cellular adhesion and proliferation. A higher cell proliferation was
10
11 observed when porous structures were incorporated than with fibrous structures.
12
13 P(3HO) porous patches modified with 750 nm fibres resulted in the best matrix for
14
15 C2C12 cells to proliferate .
16
17

18
19 Thus results from this study suggests that the P(3HO) porous cardiac patches
20
21 functionalized with 750 nm fibres are promising materials to support the infarcted
22
23 myocardium, due to their mechanical properties and ability to deliver cells in order to
24
25 allow efficient tissue regeneration caused by their good cell adhesion properties.
26
27

28 29 **4.4. Use of P(3HO) as a novel functional material in cardiac tissue engineering**

30
31

32 The heart wall is composed of a high density of cardiomyocytes and fibroblasts with
33
34 abundant vascular network and collagen based extracellular matrix (ECM). Native
35
36 tissue matrix serves as a structural and informational template for cell attachment and
37
38 tissue formation (Gupta *et al.*, 2006). In this work, the P(3HO) patches were proposed
39
40 as an alternative for the extra cellular matrix (ECM), therefore, their cell adhesiveness
41
42 and proliferation will directly affect number of adhered cells and hence the quality of
43
44 the engineered tissue. In this study NVRM cells were grown on both P(3HO) and
45
46 collagen and the cell attachment, viability and proliferation was compared. Our results
47
48 have shown that P(3HO) was as good as collagen in terms of cell attachment, viability
49
50 and proliferation, however, with respect to mechanical integrity, degradation rate,
51
52 processability and the fact that it is a non-animal source polymer are distinctive
53
54 advantages of the P(3HO) patches as compared to that of collagen.
55
56
57
58
59
60

1
2
3 The proper contraction of individual cardiomyocytes is essential for the normal
4 functioning of the heart. Intracellular calcium is the main factor that regulates
5 cardiomyocyte contraction. First, an action potential leads to the opening of L-Type
6 calcium channel present in the membrane of the cells. Second, the calcium entering
7 the cells triggers the release of calcium from the sarcoplasmic reticulum, leading to
8 a marked increase of cytosolic calcium concentration. High concentrations of
9 intracellular calcium initiate the interaction of contractile filaments and subsequent
10 contraction. Relaxation occurs by the removal of calcium from the cytosol by calcium
11 transporters. It has been described that Gap junctions coordinate the contraction of
12 individual cardiomyocytes and this force is transduced to the extracellular matrix,
13 which coordinates the overall contraction of the heart (Harvey and Leinwand 2011).
14 Engler *et al.*, (2008) have shown that the culturing of embryonic cardiomyocytes on a
15 series of substrates of different elasticity has a significant effect in the transmission of
16 contractile function and that cells in a rigid matrix are deficient in the assembly of
17 contractile proteins and their beating frequency slows down over time (Engler *et al.*,
18 2008). As a result, the extracellular matrix to which cardiomyocytes attach is a key
19 factor for a highly regulated system such as the heart. In order to analyze the effect of
20 P(3HO) on isolated cardiomyocyte contraction, fresh cardiomyocytes were seeded on
21 P(3HO) coated cover slips and the effect of a range of frequencies on the
22 cardiomyocyte contraction was examined. Results show that no significant
23 differences were observed between the polymer and the control in terms of
24 contraction and relaxation velocities expressed as 'time to peak 90%' and 'time to
25 baseline 50%' respectively or for the amplitude of contraction (% shortening).
26 Decreased function of individual cardiomyocyte contraction is known to lead to the
27 deterioration of cardiac performance. Our results showed that the polymer maintains
28
29
30
31
32
33
34
35
36
37
38
39
40
41
42
43
44
45
46
47
48
49
50
51
52
53
54
55
56
57
58
59
60

1
2
3 the effect of frequency on cardiomyocytes. When the frequency of the electrical
4
5 impulse was increased from 5 to 0.5 seconds, the cardiomyocyte contraction
6
7 decreased significantly in the control, which is the normal response in adult rat cells,
8
9 but less so on the polymer. There was no significant difference in response between
10
11 with and without polymer, although there was a tendency for contraction to be
12
13 improved on the polymer.
14
15

16
17 As described before, calcium is a central regulator of cardiac contractibility. We have
18
19 studied the effect of increasing calcium concentrations on cardiomyocyte contraction.
20
21 It has been shown that an intracellular calcium increment leads to an increment in the
22
23 force of contraction that results in a higher contraction amplitude until a saturation
24
25 point at which no further increment in contraction occurs (Bers 2000). Our results
26
27 showed that no significant differences were observed between the polymer and the
28
29 control in terms of 'time to peak 90%', 'time to baseline 50%' and amplitude of
30
31 contraction (% shortening). As expected, an increment in cardiomyocyte contraction
32
33 was observed when the concentration of calcium was increased from 1mM to 2mM
34
35 on both the polymer sample and the control, reaching a point of maximum
36
37 contraction. These results showed that the polymer maintains the effect of calcium
38
39 and hence the functionality of the cardiac tissue.
40
41
42
43

44
45 Our results suggest that P(3HO) supported the maintenance of the contraction of adult
46
47 cardiomyocytes and hence is a promising novel material to support the heart during
48
49 the regeneration process without interfering with the cardiomyocytes' performance.
50
51 Hence, P(3HO) is a potential novel healthcare material that can be effectively used in
52
53 myocardial tissue engineering.
54
55

56 **4.5. Incorporation of active molecules**

57
58
59
60

4.5.1. RGD immobilization

The fabrication of biodegradable constructs in tissue engineering is essential to provide a matrix for cell proliferation, migration and differentiation and to act as a support for the organ during regeneration. In addition to the biomaterial matrix, the control of cardiac cell environment can be enhanced by the design of biomaterials that provide adhesion, growth, migration or differentiation signals. Neat cardiac patches were further functionalised via the incorporation of active factors. It has been observed that proteins that contain the Arg-Gly-Asp (RGD) sequence are recognized by several different integrins in their adhesion protein ligands (Ruoslahti 1996). In order to allow efficient host cell recruitment and adhesion, RGD motifs were immobilized on the patches. For the RGD immobilization a series of chemical reactions were carried out to incorporate active amino terminal structures on the carboxylic acid end of the P(3HO) molecule, followed by the reaction of the terminal amine with the RGD sequence. The incorporation of the amino terminal group into the P(3HO) molecule was carried out through the addition of hexaethyleneglycol-diamine to the P(3HO) carboxylic acid end. The incorporation of the hexaethyleneglycol-diamine group to the P(3HO) was confirmed by FTIR. The appearance of a band at 3400 cm⁻¹ which corresponded to the N-H bond and the appearance of a band at 1000 cm⁻¹ showing the presence of a C-N bond suggested the presence of the hexaethyleneglycol-diamine in the P(3HO) film. In a second step, the covalent linkage of the RGD peptide to the hexaethyleneglycol-diamine present on the P(3HO) film was studied by FTIR. Results showed the presence of a strong band at 1200 cm⁻¹ corresponding to the C-N bonds that should be present in the RGD-P(3HO) polymer, due to the linkage of the hexaethyleneglycol-diamine with P(3HO) and with the RGD peptide. In addition, the disappearance of the band corresponding

1
2
3 to the NH₂ primary amine group further confirmed the formation of the RGD-
4
5 hexaethyleneglycol-diamine- P(3HO) linkage.
6
7

8 With the incorporation of RGD structures in the P(3HO) cardiac patches, an
9
10 increment in the hydrophilicity of the surface was expected (Lin *et al.*, 1992, Lin *et*
11
12 *al.*, 1994). As polar molecules interact better with water, an increment in the
13
14 molecular hydrophilicity is usually detected when RGD motifs are immobilized. The
15
16 water contact angle of the P(3HO)-RGD immobilized cardiac patches was $93.4 \pm 0.1^\circ$,
17
18 whereas that of neat P(3HO) water contact angle was $101.1 \pm 0.8^\circ$. These results thus
19
20 showed a significant decrease in the water contact angle. Hence, the expected increase
21
22 in the surface hydrophilicity after the modification with RGD peptides reconfirmed
23
24 the incorporation of the RGD peptide onto the P(3HO) film. Further, X-ray
25
26 photoelectron spectroscopy (XPS) studies will be carried out in the future for a
27
28 surface elemental analysis confirmation and tripeptide quantification.
29
30
31
32

33 In order to study any possible effect of the RGD immobilized peptides on the
34
35 mechanical properties of the P(3HO) cardiac patches, dynamic mechanical analysis
36
37 under static conditions was carried out. No differences were observed in terms of the
38
39 polymer stiffness after the RGD incorporation. However, a decrease in the tensile
40
41 strength was observed with the RGD immobilization. As the linkage of the RGD
42
43 motifs to the surface of the P(3HO) cardiac patches were carried out through
44
45 hexaethyleneglycol-diamine molecules incorporated in the polymer, differences in the
46
47 mechanical properties can be attributed to the presence of these molecules which
48
49 perhaps embedded themselves between the chains of the polymer, spacing them apart.
50
51 In agreement with our results, previous work by other groups has shown a decrease in
52
53 the tensile strength and an increment in the elongation at break when polyethylene-
54
55
56
57
58
59
60

glycol was incorporated into cellulose acetate films as a plasticizer (Yuan *et al.*, 2001). Finally, SEM images show an increment in the surface roughness after the RGD modification.

4.5.2. VEGF incorporation

As vascularisation is crucial in cardiac patches, VEGF was incorporated in order to assist cell growth and tissue vascularisation. Mechanical properties of the P(3HO)-VEGF cardiac patches were determined and compared with P(3HO) patches. Similar stiffness was obtained after the VEGF incorporation. However, a decrease in the tensile strength and an increment in the elongation at break were observed with VEGF. It is possible that VEGF molecules interact with the polymer by decreasing the chains interaction and hence decreasing the tensile strength and increasing the elongation at break by stretching the chains (Wang and Wu 2005). Although an increment in the surface hydrophilicity can be expected with the incorporation of VEGF molecules, due to an increment in the surface polarity, no significant differences were observed in terms of the surface wettability after the VEGF incorporation. The reason of this observation can be related to the amount of VEGF incorporated, which was too low to have an effect on the surface wettability. SEM images show a slight increment in the surface roughness in P(3HO)-VEGF cardiac patches. Surface roughness studies should be carried out in future for a quantitative analysis.

4.5.3. *In vitro* cell proliferation in P(3HO) cardiac patches containing VEGF and RGD peptide

C2C12 myoblast cells were seeded on P(3HO) cardiac patches containing VEGF, P(3HO) cardiac patches containing RGD and P(3HO) cardiac patches containing both VEGF and RGD. Cell proliferation was evaluated at 24 hrs with the MTT

1
2
3 colorimetric assay. Results showed a significant increment in the cell proliferation
4
5 when VEGF or RGD were incorporated in comparison to P(3HO) patches. In terms of
6
7 RGD, these results suggested that as previously reported in literature, the increased
8
9 cell-polymer interactions play a pivotal role in simulating cell proliferation (Neff *et*
10
11 *al.*, 1999). Yoon *et al.*, (2003) showed a significant increment in cell attachment when
12
13 bone marrow stem cells isolated from rat were seeded on PLGA films immobilized
14
15 with RGD motifs (Yoon *et al.*, 2003). On the other hand, VEGF has also been shown
16
17 to have a positive effect in cell proliferation. These results are in agreement with
18
19 previous reports that show the presence of VEGF receptors, which were thought to be
20
21 present exclusively in endothelial cells, in a number of different cell types (Couper *et*
22
23 *al.*, 1997, Pancholi and Earle 2000, Shen *et al.*, 1993). Sipahigil *et al.*, (2012) showed
24
25 a significant increment in L-929 cell line proliferation with VEGF incorporation in
26
27 poly(lactic-co-glycolic acid) microspheres and a direct relation was observed between
28
29 VEGF concentration and % cell proliferation (Sipahigil *et al.*, 2012). Additionally,
30
31 our results showed a slightly higher increment in cell proliferation with VEGF than
32
33 with RGD incorporation. However, from these results it is not possible to conclude if
34
35 the higher effect on cell proliferation with VEGF is due to the difference in the actual
36
37 effects of this factor on the cells or due to the different amounts of VEGF and RGD
38
39 used in this study as the VEGF amount incorporated in each film was 2 μ g and in the
40
41 case of the RGD, each film was reacted with a 1.5 nmoles/ml RGD solution. Finally,
42
43 when both VEGF and RGD were incorporated, a synergistic effect was observed,
44
45 with an increment in cell proliferation by 7 times with respect to P(3HO) patches.
46
47 These results suggested that there is no interference of VEGF with RGD proteins and,
48
49 hence, both can be incorporated together to achieve better conditions that mimic the
50
51
52
53
54
55
56
57
58
59
60

1
2
3 extracellular matrix structure in the tissue, encouraging cell attachment and
4
5 proliferation.
6

7 8 4.5.4. VEGF release 9

10 The drug release profiles of VEGF loaded P(3HO) cardiac patches were studied for a
11 period of 30 days. The results obtained showed a biphasic VEGF release profile, with
12 an initial burst release followed by controlled release. On day 30 only 50% of the
13 drug was released from the cardiac patches indicating a sustained drug release for
14 periods longer than 30 days, an advantage for long term release. This controlled
15 release can be attributed to the interaction of VEGF with P(3HO) and slow
16 degradation times of PHAs in contrast to most synthetic polymers such as PLGA,
17 which undergoes bulk degradation (Weng *et al.*, 2011). In this case, due to the short
18 biological half-life and the high tumorigenic potential of VEGF, a sustained release
19 over a 30 day period is crucial to maintain a continuous stimulation, an essential
20 feature to control the amount of released factor. This was successfully achieved with
21 P(3HO) cardiac patches (Faranesh *et al.*, 2004). In conclusion, functionalised patches
22 containing RGD and VEGF proteins can create a perfect microenvironment that
23 would induce vascularization and improve cell-matrix and cell-cell interactions to
24 promote the assembly of a functional heart tissue and enhance the therapeutic
25 effectiveness of cardiac patches.
26
27
28
29
30
31
32
33
34
35
36
37
38
39
40
41
42
43
44

45 46 4.6. Conclusions 47

48
49 The replacement of infarcted cardiac tissue with engineered extracellular matrix that
50 provides mechanical and structural support allowing cell adhesion and proliferation
51 remains elusive. Our studies show a novel promising biodegradable, flexible and
52 elastomeric functional material for cardiac tissue engineering that has not been
53
54
55
56
57
58
59
60

1
2
3 explored before. In contrast to most of the material explored so far (Table 3), P(3HO)
4
5 showed similar mechanical properties to that of myocardial muscle, ideal to maintain
6
7 coordinated cardiac beating allowing support of the organ during the regeneration
8
9 process. This is also supported by our results that show no interference of P(3HO)
10
11 with cardiomyocyte performance. Additionally, as a biodegradable material, P(3HO)
12
13 degradation will allow new tissue formation with no remaining material after the
14
15 regeneration process. Furthermore, this work has shown that the addition of pores,
16
17 fibre structures and active molecules, such as RGD and VEGF, to the fabricated
18
19 cardiac patches, are strong environmental cues that imitate the cardiac extracellular
20
21 matrix structure in the tissue and enhance cell adhesion and proliferation. In this case,
22
23 the P(3HO) chemical structure allowed the successful covalent bonding of RGD
24
25 tripeptides and incorporation of VEGF, that showed a favorable sustained release.
26
27 This work has proven for the first time, the great distinctive features of P(3HO) for
28
29 cardiac tissue engineering. Future work will involve detailed studies involving the
30
31 incorporation of co-monomers into the polymer backbone to allow further fine tuning
32
33 of the Poly(3-hydroxyalkanoate) properties for myocardial tissue engineering
34
35 applications.
36
37
38
39
40
41
42
43
44

45 References

- 46
47 Balguid A, Mol A, van Marion M, Bank R, Bouten C, Baaijens F. 2009, Tailoring
48
49 fiber diameter in electrospun poly(epsilon-caprolactone) scaffolds for optimal cellular
50
51 infiltration in cardiovascular tissue engineering, *Tissue Eng Part A*, 15(2): 437-44.
52
53
54
55 Bers D. 2000, Calcium Fluxes Involved in Control of Cardiac Myocyte Contraction,
56
57 *Circ Res*, 87: 275-281.
58
59
60

1
2
3 Boland E, Wnek G, Simpson D, Pawlowski K, Bowlin G. 2001, Tailoring tissue
4 engineering scaffolds using electrostatic processing techniques: a study of
5 poly(glycolic acid) electrospinning, *J Macromol Sci Pure Appl Chem*, 38(12): 1231–
6
7 43.
8
9

10
11
12 Chen M, Patra P, Warner S, Bhowmick S. 2007, Role of fiber diameter in adhesion
13 and proliferation of NIH 3T3 fibroblast on electrospun polycaprolactone scaffolds,
14
15 *Tissue Eng*, 13(3): 579-87.
16
17

18
19 Chen Q, Harding S, Ali N, Jawad H, Boccaccini A. 2008, Cardiac tissue engineering.
20
21 *Tissue Engineering Using Ceramics and Polymers*, Woodhead, CRC Pr.
22
23

24
25 Couper L, Bryant S, Eldrup-Jorgensen J, Bredenberg C, Lindner V. 1997, Vascular
26 endothelial growth factor increases the mitogenic response to fibroblast growth
27 factor-2 in vascular smooth muscle cells *in vivo* via expression of fms-like tyrosine
28 kinase-1, *Circ Res*, 81: 932–939.
29
30
31

32
33
34 Drury J, Dennis R, Mooney D. 2004, The tensile properties of alginate hydrogels,
35
36 *Biomaterials*, 25(16): 3187–3199.
37
38

39
40 Eichhorn S, Sampson W. 2005, Statistical geometry of pores and statistics of porous
41 nanofibrous assemblies, *J R Soc Interface*, 2: 309–318.
42
43

44
45 Engler A, Carag-Krieger C, Johnson C, Raab M, Tang H, Speicher D, Sanger J,
46
47 Sanger J and Discher D. 2008, Embryonic cardiomyocytes beat best on a matrix with
48 heart-like elasticity: scar-like rigidity inhibits beating, *J Cell Sci*, 121: 3794–3802.
49
50

51
52 Eshraghi S, Das S. 2010, Mechanical and microstructural properties of
53 polycaprolactone scaffolds with one-dimensional, two-dimensional, and three-
54
55
56
57
58
59
60

1
2
3 dimensional orthogonally oriented porous architectures produced by selective laser
4 sintering, *Acta Biomater*, 6(7): 2467-76.

5
6
7
8 Faranesh A, Nastley M, Perez de la Cruz C, Haller M, Laquerriere P, Leong K,
9 McVeigh E. 2004, *In Vitro* release of Vascular Endothelial Growth Factor From
10 Gadolinium-Doped Biodegradable Microspheres, *Magnetic Reson Med*, 51: 1265–
11 1271.

12
13
14
15
16
17
18 Flemming R, Murphy C, Abrams G, Goodman S, Nealey P. 1999, Effects of synthetic
19 micro and nano-structures surfaces on cell behaviour, *Biomaterials*, 20, 573-588.

20
21
22
23
24
25
26
27
28
29
30
31
32
33
34
35
36
37
38
39
40
41
42
43
44
45
46
47
48
49
50
51
52
53
54
55
56
57
58
59
60

Garlotta D. 2001, Literature review of poly(lactic acid), *J Polym Environ*, 9(2): 63–
84.

Giraud M, Armbruster C, Carrel T, Tevæarai H. 2007, Current state of the art in
myocardial tissue engineering, *Tissue Eng*, 13: 1825-1836.

Goldstein A, Zhu G, Morris G, Meszlenyi R, Mikos A. 1995, Effect of osteoblastic
culture conditions on the structure of poly(DL-lactic-co-glycolic acid) foam scaffolds,
Tissue Eng, 5: 421-433.

Guan J, Fujimoto K, Sacks M, Wagner W. 2005, Preparation and characterization of
highly porous, biodegradable polyurethane scaffolds for soft tissue applications.
Biomaterials, 26(18): 3961–3971.

Guan J, Fujimoto K, Wagner W. 2008, Elastase-Sensitive Elastomeric Scaffolds with
Variable Anisotropy for Soft Tissue Engineering, *Pharm. Res.*, 25(10): 2400–2412.

Gupta V, Grande-Allen K. 2006, Effects of static and cyclic loading in regulating
extracellular matrix synthesis by cardiovascular cells, *Cardiovasc Res*, 72, 375–383.

1
2
3 Harvey P and Leinwand L. 2011, Cellular mechanisms of cardiomyopathy, *J cell biol*,
4
5 194: 3 355-365.
6

7
8 Hersel U, Dahmen C, Kessler H. 2003, RGD modified polymers: biomaterials for
9
10 stimulated cell adhesion and beyond, *Biomaterials*, 24: 4385–4415.
11

12 Hocking P, Marchessault R. 1994, Biopolyesters, Chemistry and Technology of
13
14 Biodegradable Polymers, *London: Chapman and Hall*. Academic Pr.
15

16
17 Hsia H, Nair M, Mintz R, Corbett S. 2011, The fibre diameter of synthetic
18
19 bioresorbable extracellular matrix influences human fibroblast morphology and
20
21 fibronectin matrix assembly, *Plast Reconst Surg*, 127(6): 2312–2320.
22
23

24
25 Jawad H, Lyon A, Harding S, Ali N and Boccaccini A. 2008, Myocardial tissue
26
27 engineering, *Br Med Bull*, 87: 31–47.
28

29
30 Jell G, Minelli C, Stevens M. 2009, Biomaterial-Related Approaches: Surface
31
32 Structuring. *Fundamentals of Tissue Engineering and Regenerative Medicine*.
33
34 Springer, 469-484.
35

36
37 Krupnick A, Kreisel D, Szeto W, Popma S, Rosengard B. 2001, A murine model of
38
39 left ventricular tissue engineering, *J Heart Lung Transplant*, 20: 197–198.
40

41 Lampin R, Warocquier-Cle'roux, Legris C, Degrange M, Sigot-Luizard F. 1997,
42
43 Correlation between substratum roughness and wettability, cell adhesion, and cell
44
45 migration, *J Biomed Mater Res*, 36(1): 99-108.
46
47

48
49 Lee J, Jeong S, Bae M, Yang H, Heo D, Kim C, Alsberg E, Kwon K. 2011, Highly
50
51 Porous Electrospun Nanofibers Enhanced by Ultrasonication for Improved Cellular
52
53 Infiltration, *Tissue Eng Part A*, 17: 21-22.
54
55

1
2
3 Lebourg M, Sabater Serra R, Más Estellés J, Hernández Sánchez F, Gómez Ribelles
4 JL, Suay Antón J. 2008, Biodegradable polycaprolactone scaffold with controlled
5 porosity obtained by modified particle-leaching technique, *J Mater Sci Mater Med*,
6
7 19(5): 2047-53.

8
9
10
11 Lee Y, Park S, Lee W, Ko J, Kim H. 2003, MG63 osteoblastic cell adhesion to the
12 hydrophobic surfaceprecoated with recombinant osteopontin fragments, *Biomaterials*,
13
14 24: 1059–1066.

15
16
17 Li D. 2011, Encyclopedia of Microfluidics and Nanofluidics, *Springer*.

18
19
20
21
22 Li W, Laurencin C, Caterson E, Tuan R, Ko F. 2002, Electrospun nanofibrous
23 structure: A novel scaffold for tissue engineering, *J Biomed Mater Res*, 15;60(4):
24
25 613-21.

26
27
28
29
30 Lin H, Garciaecheverria C, Asakura S, Sun W, Mosher D, Cooper S. 1992,
31 Endothelial-cell adhesion on polyurethanes containing covalently attached RGD-
32 peptides, *Biomaterials*, 13: 905–14.

33
34
35
36
37 Lin H, Sun W, Mosher D, Garciaecheverria C, Schaufelberger K, Lelkes P, Cooper S.
38 1994, Synthesis, surface, and cell adhesion properties of polyurethanes containing
39 covalently grafted RGD-peptides, *J Biomed. Mater Res*, 28: 329–42.

40
41
42
43
44 Lu X , and Chung D. 1998, A comparative study of the wettability of steel, carbon,
45 and polyethylene fibres by water, *Cement and Concrete Research*, 28(6): 783–786.

46
47
48
49
50 Ma Y, Yang D, Shi W, Li S, Fan Z, Tu J, Wang W. 2012, Preparation and properties
51 of novel poly(propylene oxide)-block-poly(lactide)-based polyurethane foams. *Polym.*
52
53 *Eng. Sci*, 53(2):343-352.

- 1
2
3 Morosco J. 2002, Conquering heart disease: a call to action, *Prev Cardiol*, 5: 31– 6.
4
5 Mosmann T. 1983, Rapid colorimetric assay for cellular growth and survival:
6
7 Application to proliferation and cytotoxicity assays, *J. Immunol Methods*, 65(1–2):
8
9 55–63.
10
11
12 Nagueh S, Shah G, Wu Y, Torre-Amione G, King N, Lahmers S. 2004, Altered titin
13
14 expression, myocardial stiffness and left ventricular function in patients with dilated
15
16 cardiomyopathy, *Circulation*, 110: 155-162.
17
18
19 Neff J, Tresco P, Caldwell K. 1999, Surface modification for controlled studies of
20
21 cell-ligand interactions, *Biomaterials*, 20(23-24): 2377-93.
22
23
24 Nelson T, Kaufman E, Kline J, Sokoloff L. 1981, The extraneural distribution of
25
26 hydroxybutyrate, *J Neurochem*, 37: 1345-1348.
27
28
29
30 Pancholi S, Earle K. 2000, Pattern of angiogenic cytokine release from human
31
32 vascular smooth muscle cells programmed by amino acid deprivation, *Cytokine*, 12:
33
34 1322–1325.
35
36
37 Perry E, Roth J. 2003, Cardiovascular tissue engineering: constructing living tissue
38
39 cardiac valves and blood vessels using bone marrow, umbilical cord blood, and
40
41 peripheral blood cells, *J Cardiovasc Nurs*, 18: 30.
42
43
44
45 Rai R, Yunos D, Boccaccini A, Knowles J, Barker I, Howdle S, Tredwell G,
46
47 Keshavarz T, and Roy I. 2011, Poly-3-hydroxyoctanoate P(3HO), a Medium Chain
48
49 Length Polyhydroxyalkanoate Homopolymer from *Pseudomonas mendocina*,
50
51 *Biomacromolecules*, 13;12(6): 2126-2136.
52
53
54
55
56
57
58
59
60

1
2
3 Rezania A, Healy K. 2008, Biomimetic Peptide Surfaces That Regulate Adhesion,
4 Spreading, Cytoskeletal Organization, and Mineralization of the Matrix Deposited by
5 Osteoblast-like Cells, *Biotechnology Progress*, 15(1): 19-32.
6
7

8
9 Richert L, Vetrone F, Yi J, Zalzal S, Wuest J, Rosei F, and Nanci A. 2008, Surface
10 Nanopatterning to Control Cell Growth, *Adv. Biomater*, 20: 8, 1488-1492.
11
12

13
14 Roeder B, Kokini K, Sturgis J, Robinson J, Voytik-Harbin S. 2002, Tensile
15 mechanical properties of three-dimensional type I collagen extracellular matrices with
16 varied microstructure, *J. Biomech. Eng*, 124(2): 214-22.
17
18

19
20 Ruoslahti E. 1996, RGD and other recognition sequences for integrins, *Ann Rev Cell*
21 *Dev Bio*, 12: 697-715.
22
23

24
25
26
27 Santerre JP, Woodhouse K, Laroche G, Labow R. 2005, Understanding the
28 biodegradation of polyurethane: From classical implants to tissue engineering
29 materials, *Biomaterials*, 26(35): 7457-7470.
30
31

32
33
34 Shen H, Clauss M, Ryan J, Schmidt A, Tjiburg P, Borden L, Connolly D, Stern D,
35 Kao J. 1993, Characterization of vascular permeability factor/vascular endothelial
36 growth factor receptors on mononuclear phagocytes, *Blood*, 81: 2767-2773.
37
38

39
40 Shin M, Ishii O, Sueda T, Vacanti J. 2004, Contractile cardiac grafts using a novel
41 nanofibrous mesh, *Biomaterials*, 25: 3717-3723.
42
43

44
45
46
47 Silvestri A, Boffito M, Sartori S, Ciardelli G. 2013, Biomimetic Materials and
48 Scaffolds for Myocardial Tissue Regeneration, *Macromol Biosc*, 13(8):948-1019.
49
50

51
52
53 Silvestri A, Sartori S, Boffito M, Clara Mattu, Di Rienzo A, Boccafoschi F, Ciardelli
54 G. 2014, Biomimetic myocardial patches fabricated with poly(E-caprolactone) and
55
56
57
58
59
60

1
2
3 polyethylene glycol-based polyurethanes, *J Biomed Mater Res B Appl Biomater*,
4
5 102(5):1002-13.
6
7

8 Sipahigil O, Alarçin E, Türko lu M, Dortunç B, Karagöz H, Ülkür E, Vural M, Çapan
9 Y. 2012, Characterization, cell proliferation and cytotoxicity evaluation of vascular
10 endotelial growth factor loaded poly(lactic-co-glycolic acid) microspheres, *Nobel*
11 *Med*, 8(1): 77-82.
12
13
14
15
16

17
18 Sutton M and Sharpe N. 2000, Left Ventricular Remodeling After Myocardial
19 Infarction: Pathophysiology and Therapy, *Circulation*, 101: 2981-2988.
20
21
22

23 Wang J, Wu W. 2005, Swelling behaviors, tensile properties and thermodynamic
24 studies of water sorption of 2-hydroxyethyl methacrylate/epoxy methacrylate
25 copolymeric hydrogels, *Eur Polym J*, 41: 1143–1151.
26
27
28
29

30 Wang Y, Ruan L, Lo W, Chua H, Yu H. 2006, Construction of recombinant *Bacillus*
31 *subtilis* for production of polyhydroxyalkanoates, *Appl Biochem. Biotechnolo*, 129-
32 1332:1015-22.
33
34
35
36

37
38 Watanabe S, Shite J, Takaoka H, Shinke T, Imuro Y, Ozawa T, Otake H, Matsumoto
39 D, Ogasawara D, Paredes O and Yokoyama M. 2006, Myocardial stiffness is an
40 important determinant of the plasma brain natriuretic peptide concentration in patients
41 with both diastolic and systolic heart failure, *European Heart J*, 27, 832–838.
42
43
44
45
46

47 Webb A, Yang J, Ameer G. 2004, Biodegradable polyester elastomers in tissue
48 engineering, *Expert Opin Biol Ther*, 4(6): 801-12.
49
50
51

52
53 Weng Y, Wang X, Wang Y. 2011, Biodegradation behaviour of PHAs with different
54 chemical structures under controlled composting conditions, *Polymer testing*, 30: 372-
55 380.
56
57
58
59
60

1
2
3 Williams S, Martin D, Horowitz D, Peoples O. 1999, PHA applications: addressing
4 the price performance issue. I. Tissue engineering, *Int J Biol Macromol*, 25: 111–121.
5
6

7
8 Yoon J, Song S, Lee D, Park T. 2003, Immobilization of cell adhesive RGD peptide
9 onto the surface of highly porous biodegradable polymer scaffolds fabricated by gas
10 foaming/salt leaching method, *Biomaterials*, 25: 5613-5620
11
12

13
14
15 Yuan J, Shang P, Wu S. 2001, Effects of Polyethylene Glycol on Morphology,
16 Thermomechanical Properties, and Water Vapor Permeability of Cellulose Acetate–
17 Free Films, *Pharm Technol*, 25(10): 62-74.
18
19

20
21 Zinn, M, Witholt B, and Egli T. 2001, Occurrence, synthesis and medical application
22 of bacterial polyhydroxyalkanoate, *Adv Drug Delivery, Rev.* 53, 5-21.
23
24
25
26
27
28
29

30 **Figure 1.** The percentage cell proliferation of C2C12 cell line normalized against cell
31 growth on tissue culture plastic (n=4; error bars=±SD). Mean ± sem, n=4. An
32 increment in fibre diameter resulted in a significant increment in % cell proliferation,
33 One-way ANOVA P<0.05.
34
35
36
37
38

39 **Figure 2.** The % cell proliferation of C2C12 cell line on neat P(3HO) patches
40 containing porous structures, fibrous structures and both fibrous and porous
41 structures. Results were normalized against cell growth results on tissue culture
42 plastic, used as a control. Mean ± sem, n=4. % cell proliferation was significantly
43 greater when porous or fibres were incorporated on to the P(3HO) patches, One-way
44 ANOVA P<0.01.
45
46
47
48
49
50
51
52
53
54
55
56
57
58
59
60

1
2
3 **Figure 3.** SEM images of C2C12 cells at 24 hr on P(3HO) A) neat polymer patches,
4 B) porous patches C) neat polymer patches modified with 750 nm fibres and D)
5 porous patches modified with 750 nm fibres.
6
7
8
9

10 **Figure 4.** Number of live/dead NVRM cells two days after plating on P(3HO) patches
11 and collagen. Mean \pm sem, n=3 experiments. No significant differences were
12 observed between the number of live/dead cells on P(3HO) and collagen.
13
14
15
16

17 **Figure 5.** Confocal microscopy images of NVRM cells grown on P(3HO) labeled
18 with (A) ethidium homodimer-1 (B) immunofluorescent anti α -actinin and DAPI (C)
19 NVRMs grown on collagen (as a control) stained with ethidium homodimer-1. For
20 figures A and C green indicates live cells while red depicts the dead cells.
21
22
23
24
25
26

27 **Figure 6. (A)** Normalised contraction amplitude (% shortening) of adult rat
28 cardiomyocytes at different beating frequencies on P(3HO) polymer or glass cover-
29 slips. Mean \pm sem, n=5 cells from separate preparations. 2 way ANOVA shows a
30 significant effect of frequency $P < 0.001$ but no difference between P(3HO) and
31 control. **(B)** Normalised contraction amplitude (% shortening) of adult rat
32 cardiomyocytes with increasing extracellular calcium on P(3HO) polymer or glass
33 cover-slips. Mean \pm sem, n=5 cells (control) and 3-4 cells (polymer) from separate
34 preparations. No significant differences between P(3HO) and control.
35
36
37
38
39
40
41
42
43
44
45

46 **Figure 7.** The % cell proliferation of C2C12 cell line at 24 hr on P(3HO), VEGF,
47 RGD and VEGF+RGD modified P(3HO) patches. Mean \pm sem, n=4. % cell
48 proliferation significantly greater when VEGF or RGD were incorporated to the
49 P(3HO) patches, One -Way ANOVA.
50
51
52
53
54
55
56
57
58
59
60

Table 1. Fibre and particle diameters obtained by electrospinning of different solutions of P(3HO) in acetone. Values are shown \pm standard deviation.

P(3HO) concentration (wt%)	Fibre diameter (nm)	Particle diameter (nm)
1.2	750 \pm 130	-
1	700 \pm 100	-
0.7	630 \pm 100	-
0.6	370 \pm 90	-
0.5	340 \pm 100	660 \pm 60
0.2	-	580 \pm 120

Table 2. ‘time to peak 90%’ and time to ‘relaxation 50%’ when cardiomyocytes were stimulated at a range of electrical pulses of 50 V for 2 ms at 2, 5, 2, 1 and 0.5 second interval. Results are shown \pm SD. **(B)** ‘time to peak 90%’ and time to ‘relaxation 50%’ when cardiomyocytes were stimulated at a range of electrical pulses of 50 V for 2 ms at 2 second interval when calcium concentration was increased from 1 to 2, 3 and 4 mM. Results are shown \pm SD.

(A)

Intervals (sec)	Time to peak 90% (sec)		Time to baseline 50% (sec)	
	Control \pm SD	Polymer \pm SD	Control \pm SD	Polymer \pm SD
2	0.058 \pm 0.011	0.051 \pm 0.010	0.118 \pm 0.011	0.105 \pm 0.011
5	0.060 \pm 0.017	0.056 \pm 0.013	0.132 \pm 0.019	0.114 \pm 0.013
2	0.056 \pm 0.018	0.053 \pm 0.013	0.109 \pm 0.018	0.113 \pm 0.015
1	0.049 \pm 0.007	0.053 \pm 0.011	0.098 \pm 0.008	0.109 \pm 0.012
0.5	0.047 \pm 0.008	0.050 \pm 0.009	0.095 \pm 0.022	0.107 \pm 0.033

(B)

Calcium (mM)	Time to peak 90% (sec)		Time to baseline 50% (sec)	
	Control \pm SD	Polymer \pm SD	Control \pm SD	Polymer \pm SD
2	0.052 \pm 0.009	0.055 \pm 0.010	0.101 \pm 0.010	0.113 \pm 0.010
3	0.059 \pm 0.008	0.053 \pm 0.007	0.112 \pm 0.009	0.115 \pm 0.008
4	0.058 \pm 0.010	0.049 \pm 0.010	0.111 \pm 0.011	0.132 \pm 0.018

Table 3. Mechanical properties of materials proposed for myocardial tissue engineering

Polymer	Young's modulus	Tensile strength	References
Collagen	2-22 KPa	1-9 KPa	Roeder <i>et al.</i> , 2002
Alginate	10-50 KPa	10-40 KPa	Drury <i>et al.</i> , 2004
PGA	7-10 GPa	70 MPa	Webb <i>et al.</i> , 2004
PCL	343.9-364.3 MPa	10.5-16.1MPa	Eshraghi and Das 2010
PLA	1-4 GPa	30-80 MPa	Garlotta 2001
PLGA	67 MPa	4 MPa	Lin <i>et al.</i> , 2011
Myocardium (human)	0.02-0.5 MPa	3-15 KPa	Watanabe <i>et al.</i> , 2006 Nague <i>et al.</i> , 2004

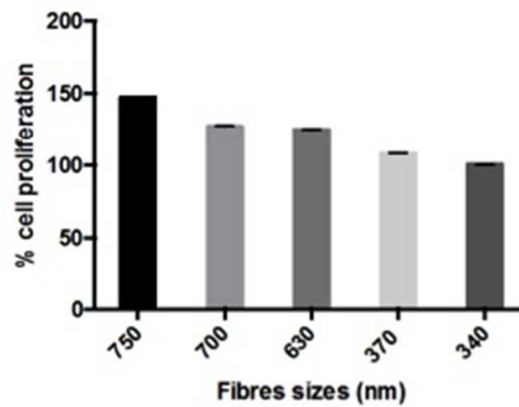


Figure 1. The percentage cell proliferation of C2C12 cell line normalized against cell growth on tissue culture plastic (n=4; error bars=±SD). Mean ± sem, n=4. An increment in fibre diameter resulted in a significant increment in % cell proliferation, One-way ANOVA $P < 0.05$.

Figure 1

94x73mm (72 x 72 DPI)

Peer Review

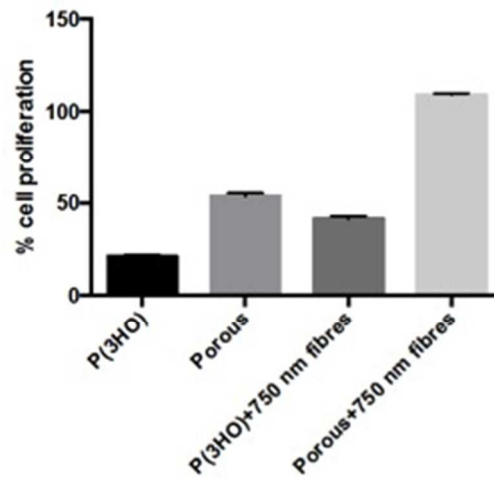


Figure 2. The % cell proliferation of C2C12 cell line on neat P(3HO) films containing porous structures, fibrous structures and both fibrous and porous structures. Results were normalized against cell growth results on tissue culture plastic, used as a control. Mean \pm sem, $n=4$. % cell proliferation was significantly greater when porous or fibres were incorporated on to the P(3HO) films, One-way ANOVA $P<0.01$.

Figure 2
90x85mm (72 x 72 DPI)

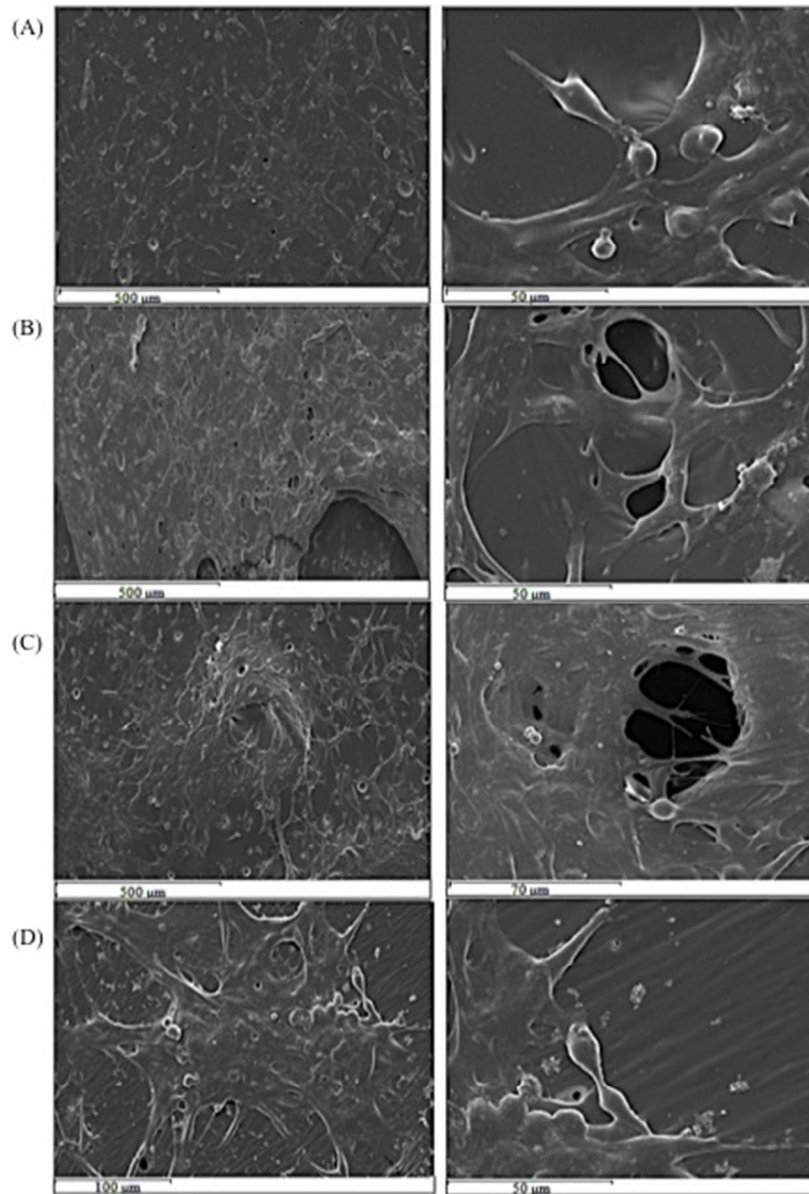


Figure 3. SEM images of C2C12 cells at 24 hr on P(3HO) A) neat polymer patches, B) porous patches C) neat polymer patches modified with 750 nm fibres and D) porous patches modified with 750 nm fibres.

Figure 3

155x225mm (72 x 72 DPI)

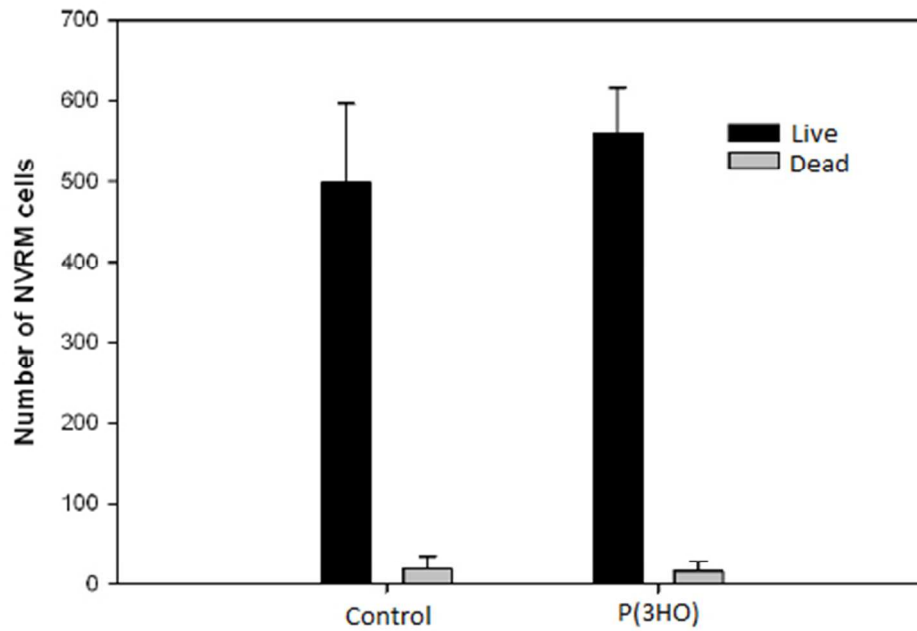


Figure 4. Number of live/dead NVRM cells two days after plating on P(3HO) patches and collagen. Mean \pm sem, n=3 experiments. No significant differences were observed between the number of live/dead cells on P(3HO) and collagen.

Figure 4
140x96mm (96 x 96 DPI)

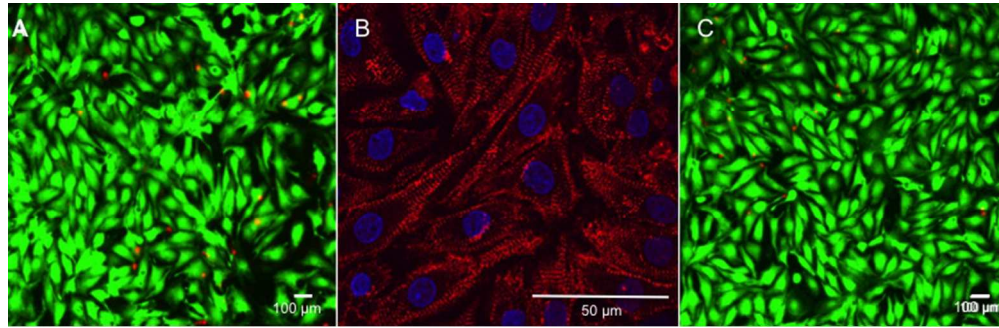


Figure 5. Confocal microscopy images of NVRM cells grown on P(3HO) labeled with (A) ethidium homodimer-1 (B) immunofluorescent anti α -actinin and DAPI (C) NVRMs grown on collagen (as a control) stained with ethidium homodimer-1. For figures A and C green indicates live cells while red depicts the dead cells.

Figure 5

146x47mm (150 x 150 DPI)

Peer Review

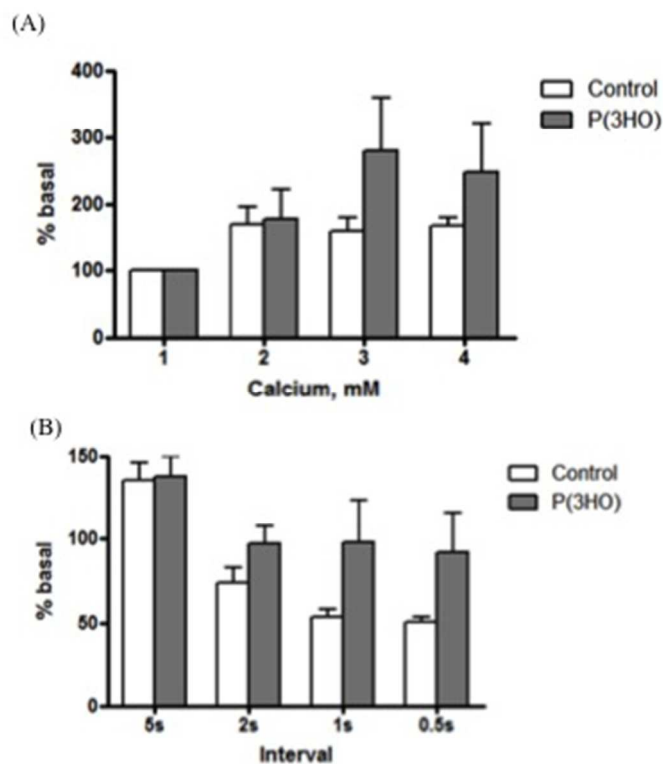


Figure 6. (A) Normalised contraction amplitude (% shortening) of adult rat cardiomyocytes at different beating frequencies on P(3HO) polymer or glass cover-slips. Mean \pm sem, $n=5$ cells from separate preparations. 2 way ANOVA shows a significant effect of frequency $P<0.001$ but no difference between P(3HO) and control. (B) Normalised contraction amplitude (% shortening) of adult rat cardiomyocytes with increasing extracellular calcium on P(3HO) polymer or glass cover-slips. Mean \pm sem, $n=5$ cells (control) and 3-4 cells (polymer) from separate preparations. No significant differences between P(3HO) and control.

Figure 6

122x138mm (72 x 72 DPI)

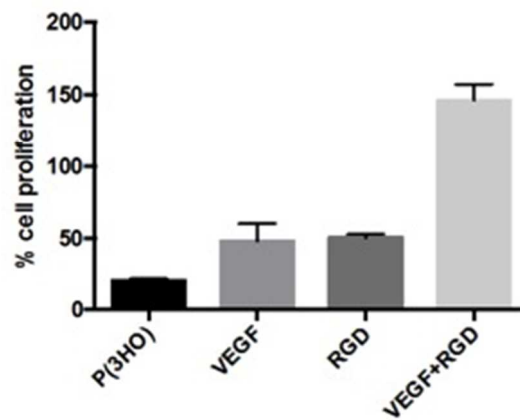


Figure 7. The % cell proliferation of C2C12 cell line at 24 hr on P(3HO), VEGF, RGD and VEGF+RGD modified P(3HO) patches. Mean \pm sem, n=4. % cell proliferation significantly greater when VEGF or RGD were incorporated to the P(3HO) films, One -Way ANOVA.

Figure 7
94x76mm (72 x 72 DPI)